Cretaceous Research 151 (2023) 105631

Contents lists available at ScienceDirect

Cretaceous Research

journal homepage: www.elsevier.com/locate/CretRes

Acynodon adriaticus from Villaggio del Pescatore (Campanian of Italy): Anatomical and chronostratigraphic integration improves phylogenetic resolution in Hylaeochampsidae (Eusuchia)

Muscioni Marco [a, 1], Alfio Alessandro Chiarenza [b, *, 1], Massimo Delfino [c, d], Matteo Fabbri [e], Kevin Milocco [a], Federico Fanti [a]

[a] Dipartimento di Scienze Biologiche, Geologiche e Ambientali, Alma Mater Studiorum, Università di Bologna, Via Zamboni 67, Bologna 40126, Italy
[b] Grupo de Ecoloxía e Bioloxía Animal, Centro de Investigacion Mariña, Universidade de Vigo, Vigo 36310, Spain
[c] Dipartimento di Scienze Della Terra, Università di Torino, Via Valperga Caluso 35, Turin 10125, Italy
[d] Institut Català de Paleontologia Miquel Crusafont, Universitat Autònoma de Barcelona, Edifici ICTA-ICP, Carrer de Les Columnes S/n, Campus de La UAB, Cerdanyola Del Vallès, Barcelona 08193, Spain
[e] Negaunee Integrative Research Center, Field Museum of Natural History, Chicago, IL, USA

ARTICLE INFO

Article history:
Received 17 February 2023
Received in revised form
3 June 2023
Accepted in revised form 21 June 2023
Available online 28 June 2023

Keywords:
Crocodylomorpha
Systematics
Bayesian
Maximum parsimony
Cretaceous
Tethys

ABSTRACT

The hylaeochampsid crocodylomorph *Acynodon adriaticus*, from the uppermost Cretaceous 'Villaggio del Pescatore' site, belongs to an early diverging lineage in Eusuchia. Here an additional specimen, MCSNT 57031, is osteologically and osteohistologically described in detail. After integrating this morphological information together with the recent chronostratigraphic recalibration of the site to the lower–middle Campanian, the tip-dated Bayesian phylogenetic analysis recovers this taxon in a monophyletic clade with the Spanish *Acynodon iberoccitanus*. Conflicting results from the maximum parsimony and Bayesian analyses, and discussion on the intraspecific variability between the specimens assigned to *A. adriaticus*, highlights the need for a detailed morphological description and integration with an updated phylogenetic scaffold, in order to resolve the monophyly of the genus *Acynodon* and the relationships of these branches of early diverging eusuchians. The curious discrepancy between morpho- and osteo-skeletal maturity suggest unique ecomorphological adaptations in this Campanian crocodylomorph.

1. Introduction

The Villaggio del Pescatore Lagerstätte (VdP hereafter), located in the municipality of Duino-Aurisina, Trieste (NE Italy), is a world-renown paleontological site due to its well-preserved Cretaceous vertebrate remains, standing out in the European palaeontological landscape (Chiarenza et al., 2021). In addition to the famous hadrosauroid *Tethyshadros insularis* (Dalla Vecchia, 2009; Chiarenza et al., 2021), remains of the small hylaeochampsid crocodylomorph *Acynodon adriaticus* were described from this site (Delfino et al., 2008a). *Acynodon* exhibits an overall bizarre morphology in comparison to other eusuchians, including a brevirostrine cranial condition: the skull is broadly similar to that of small alligatoroids (Brochu, 2010) although with larger and 'molariform' dentition. Given the bizarre morphology, fully congruent with the peak ecomorphological variation recently reported for Cretaceous crocodylomorphs by Stubbs et al. (2021), a stable phylogenetic placement of *Acynodon* in Eusuchia has been problematic (Rio and Mannion, 2021). *Acynodon* was previously considered as an example of 'archaic' alligatoroid, or one of the oldest and most primitive representatives of the entire Globidonta (Santonian–Campanian) (Buscalioni et al., 1997; Brochu, 1999, 2001, 2003; Brochu, 2003; Martin, 2007; Delfino et al., 2008a; 2008b). However, recent phylogenetic analyses place this group outside Crocodylia in the clade Hylaeochampsidae, with conflicting results regarding the monophyly of the genus (Brochu, 2011, 2012; Brochu et al., 2012; Martin et al., 2014, 2016; Jouve et al., 2019; Ristevski et al., 2020; Blanco, 2021). *Acynodon* includes three known species: *A. adriaticus*, only known from the VdP site in Italy, *A. iberoccitanus*, with referred material from Spain, southern France and Romania (with remains from these latter two countries

* Corresponding author.
E-mail addresses: a.chiarenza15@gmail.com, alfio.chiarenza@uvigo.es (A.A. Chiarenza), federico.fanti@unibo.it (F. Fanti).
[1] These authors contributed equally to this work.

https://doi.org/10.1016/j.cretres.2023.105631
0195-6671/

represented by multiple, fairly complete crania), and *A. lopezi* based on isolated teeth found in Spain (Buscalioni et al., 1997). Other occurrences of this genus come from several European locations (Delfino et al., 2008a; Blanco et al., 2020; Puértolas-Pascual et al., 2020): Muthmannsdorf (Austria), La Cabaña in Asturias (Spain), Chera (Spain), Els Nerets (Spain), Quintanilla del Coco (Spain), Laño (Spain), Arén (Spain), Massecaps (France), Quarante (France), Fox-Ampoux (France), Haţeg Basin (Romania) and VdP (Italy). Only *A. adriaticus* and *A. iberoccitanus* have been analysed in a phylogenetic context (being the material referred to *A. lopezi* not informative enough). In a context of phylogenetic uncertainty (see among others, Narváez et al., 2016; Martin et al., 2020; Blanco, 2021; Rio and Mannion, 2021), the revised chronostratigraphy of the VdP site (Chiarenza et al., 2021), type and only locality of *A. adriaticus*, offers a unique opportunity to test the phylogenetic implications of the temporal recalibration of this fossil bearing site.

This study focuses on *Acynodon adriaticus* with a comprehensive analysis of all skeletal remains ascribed to this taxon from the VdP site, discussing its age and taphonomy. Specifically, a nicely preserved individual, MCSNT 57031 (Fig. 1), assigned to the genus *Acynodon* by Delfino and Buffetaut (2006), conservatively considered as Crocodylia indet. by Delfino et al. (2008a) due to the lack of definitive autapomorphies, is herein extensively described. Here we parsimoniously refer MCSNT 57031 to *A. adriaticus* by providing an accurate anatomical description of the specimen, followed by osteohistological analysis and consideration of the palaeobiology of *A. adriaticus*. We furthermore integrate these new anatomical and chronostratigraphic information in a combined framework to improve the resolution of the genus *Acynodon* (the less inclusive clade including *Acynodon adriaticus* and *A. iberoccitanus*).

2. Institutional abbreviations

MCSNT, Museo Civico di Storia Naturale in Trieste, Italy.
MGGC, Museo Geologico Giovanni Capellini in Bologna, Italy.

3. Methods

3.1. Specimens

All crocodilian remains from the VdP were collected between 1996 and 1999 (see Table 1) and are currently housed at the Museo Civico di Storia Naturale in Trieste (MCSNT). Specimens were prepared with a chemical dissolution technique consisting in selective matrix removal with multiple formic acid baths. For this study, measurements and photographs were obtained *ex-novo* and compared with available prior measurements used in other publications (e.g. Delfino et al., 2008a, 2008b). The anatomical illustrations were preliminarily made using a microscope with integrated *camera lucida* (Leica DM 2500 P petrographic microscope with a ProgRes CFscan camera adapter), subsequently assembled with Adobe Photoshop 2020. Thin sections of rib fragments and dorsal osteoderms from MCSNT 57031 were prepared for osteohistological study and are housed in Bologna (with access numbers: MGGC 22304, 22305, 22306).

3.1.1. *New specimens assigned to* Acynodon adriaticus *and discussed in this study*

MCSNT 57031: ventrally exposed, articulated, sub-complete specimen (main focus of this study; Fig. 1); Initially described by Delfino and Buffetaut, 2006.

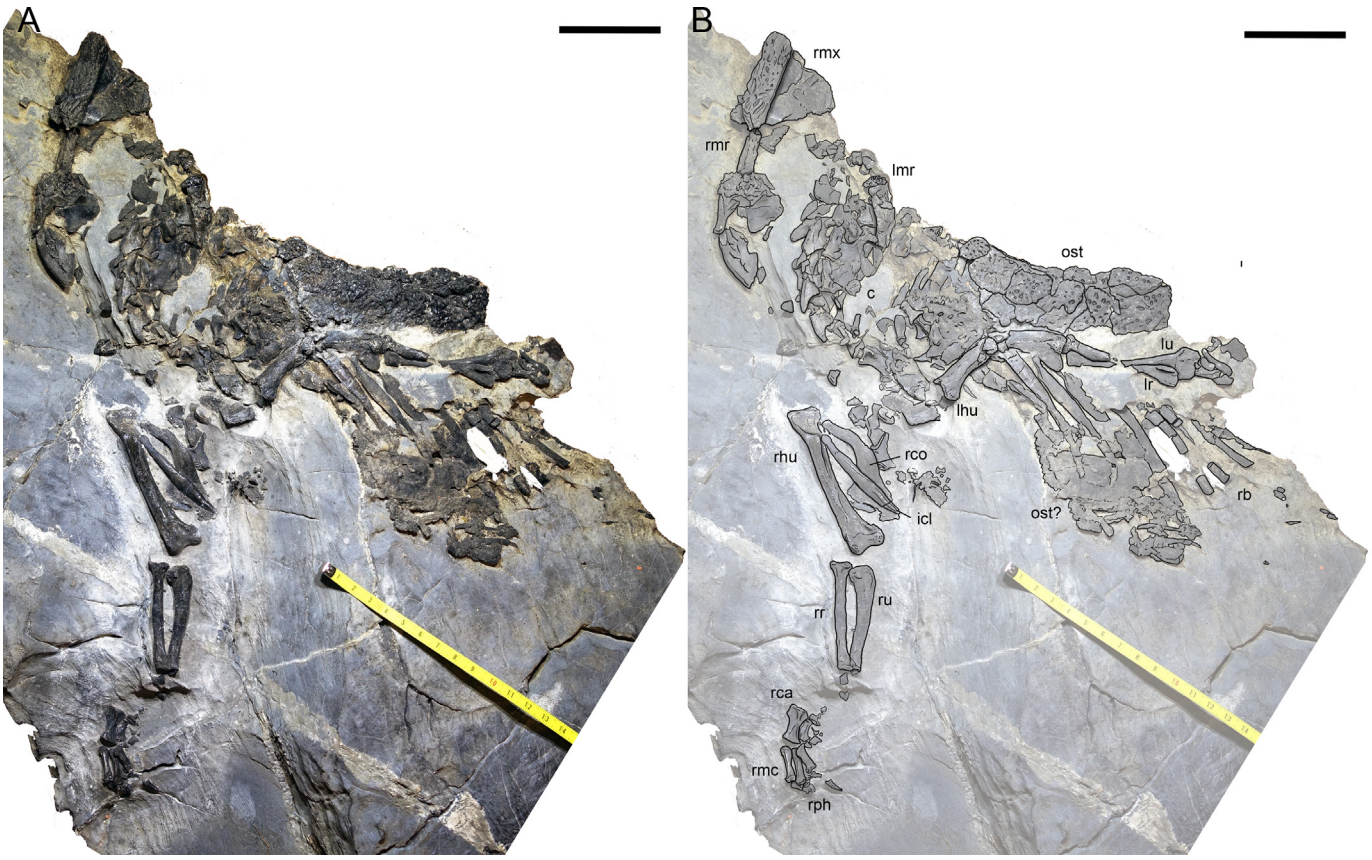

Fig. 1. Specimen of *Acynodon adriaticus* MCSNT 57031. Laminite slab with the specimen embedded in matrix (A) and anatomical elements highlighted in B. Abbreviations: c: cervical vertebrae, icl: interclavicle, lhu: left humerus, lmr: left mandibular ramus, lr: left radius, lu: left ulna, ost: osteoderms, rb: ribs, rca: radiale carpal, rco: right coracoid, rhu: right humerus, rmc: right metacarpals, rmr: right mandibular ramus, rmx: right maxilla, rph: right phalanges, rr: right radius, ru: right ulna. Scale bar: 5 cm.

Table 1
List of crocodilian remains found at the Villaggio del Pescatore site. VP, Villaggio del Pescatore, progressive numbers referring to limestone blocks quarried in order to collect vertebrate remains.

Specimen inventory	Specimen description	Quarry information
Acynodon adriaticus		
MCNST 57248	Holotype, Delfino et al., 2008a.	Collected near VP12, about 55 cm above VP1 in 1998–1999
MCNST 57032	Paratype, Delfino et al., 2008a.	Collected in the proximity of the holotype in 1996–1997
New specimens assigned to *Acynodon adriaticus* and discussed in this study		
MCSNT 57031	Ventrally exposed, articulated, sub-complete specimen.	Collected in VP4 in the same horizon as VP2 in 1996–1997
MCSNT 57245	An isolated, well preserved robust crocodilian rib laying on the flat surface of a larger matrix slab with other unidentified bone fragments. The tuberculum is shorter than the capitulum and apparently has a larger articular surface. The rib progressively thickens distally and has a wide costal cartilage articular surface.	Collected from Slab 38 in 1998–1999
MCSNT 21.S239-1.0.22 (57248a)	Six well preserved osteoderms, three of them in partial overlap. The larger ones, measured at their longer axis, are 22.8 mm, 24.5 mm and 27 mm long respectively. These osteoderms show two low keels, one straight and the other concave and larger, comparable to the condition described in the paratype by Delfino et al. (2008a).	Collected near the holotype in 1998–1999
MCSNT 21.S239–1.0.22 (57248b)	Three small osteoderms and two robust ribs in association, both showing shorter and stouter tubercula than capitula, with wider articular surfaces. The shorter rib measures 46.7 mm in length and lacks its distalmost portion; the longer one measures 57.2 mm, appears to be complete and gradually thickens at its distal end, revealing a large costal cartilage articular surface.	Collected near the holotype in 1998–1999
Specimens assigned to Crocodylomorpha indet.		
MCSNT 57033	a ~4 cm long unidentified small reptile bone, possibly a rib, exposing its sagittal section on the surface of a small laminite fragment.	Collected in the proximity of the holotype in 1998–1999
MCSNT 57035	a ~5 cm long bone element exposed on a calcareous slab with an ornamented surface, here identified as a ventrally exposed crocodilian mandibular symphysis.	Collected from Slab 41 in 1998–1999
MCSNT 57036	a ~2 cm anteroposteriorly long vertebra, possibly a fragmented cervical, three-dimensionally prepared out of the matrix.	Collected from Slab 41 in 1998–1999
MCSNT 57037	An almost unrecognizable smooth bone fragment hardly visible on a small matrix slab associated with other indeterminate vertebrate fossil material, previously tentatively identified as a fragmented ventral osteodermal surface.	Collected from Slab 15 in 1996–1997 and 1998–1999

MCSNT 21.S239-1.0.22 (57248a): six well-preserved osteoderms, three of them in partial overlap (Fig. 2A). The larger ones, measured at their longer axis, are 22.8 mm, 24.5 mm, and 27 mm long respectively. These osteoderms show two low keels, one straight and the other concave and larger, comparable to the condition described in the paratype by Delfino et al. (2008a).

MCSNT 57245: an isolated, well-preserved robust crocodilian rib laying on the flat surface of a larger matrix slab with other unidentified bone fragments. The tuberculum is shorter than the capitulum and has a larger articular surface. The rib progressively thickens distally and has a wide costal cartilage articular surface (Fig. 2B).

MCSNT 21.S239-1.0.22 (57248b): three small osteoderms and two robust ribs in association, both showing shorter and stouter tubercula than capitula, with wider articular surfaces (Fig. 2C). The shorter rib measures 46.7 mm in length and lacks its distalmost portion; the longer one measures 57.2 mm, appears to be complete and gradually thickens at its distal end, revealing a large costal articular surface.

3.1.2. Specimens assigned to Crocodylomorpha indet

MCSNT 57033: a ~4 cm long unidentified small reptile bone, possibly a rib, exposing its sagittal section on the surface of a small laminite fragment (Fig. S1A).

MCSNT 57035: a ~5 cm long bone element exposed on a calcareous slab with an ornamented surface here identified as a ventrally exposed crocodilian mandibular symphysis (Fig. S1B).

MCSNT 57036: a ~2 cm anteroposteriorly long vertebra, possibly a fragmented cervical, three-dimensionally prepared out of the matrix (Fig. S1C).

MCSNT 57037: an almost unrecognizable smooth bone fragment hardly visible on a small matrix slab associated with other indeterminate vertebrate fossil material, previously tentatively identified as a fragmented ventral osteodermal surface (Fig. S1D).

3.2. Stratigraphy and age

The VdP site is located near a dismissed quarry in the municipality of Duino Aurisina, Trieste, Italy (Fig. 3). The overall geological setting of the site and surrounding areas, including key information on facies analysis, sedimentology, paleontology, and isotope-based stratigraphy, has been described in detail in the literature (Tarlao et al., 1993, 1995; Attura, 1999; Palci, 2003; Dalla Vecchia, 2008, 2009; Chiarenza et al., 2021; Consorti et al., 2021), with a recent redescription and re-evaluation documented in Chiarenza et al. (2021). The VdP deposits originated at the northern margin of the Adriatic Carbonate Platform system (AdCP): in the area, the Upper Cretaceous to lowermost Paleocene interval is represented by two

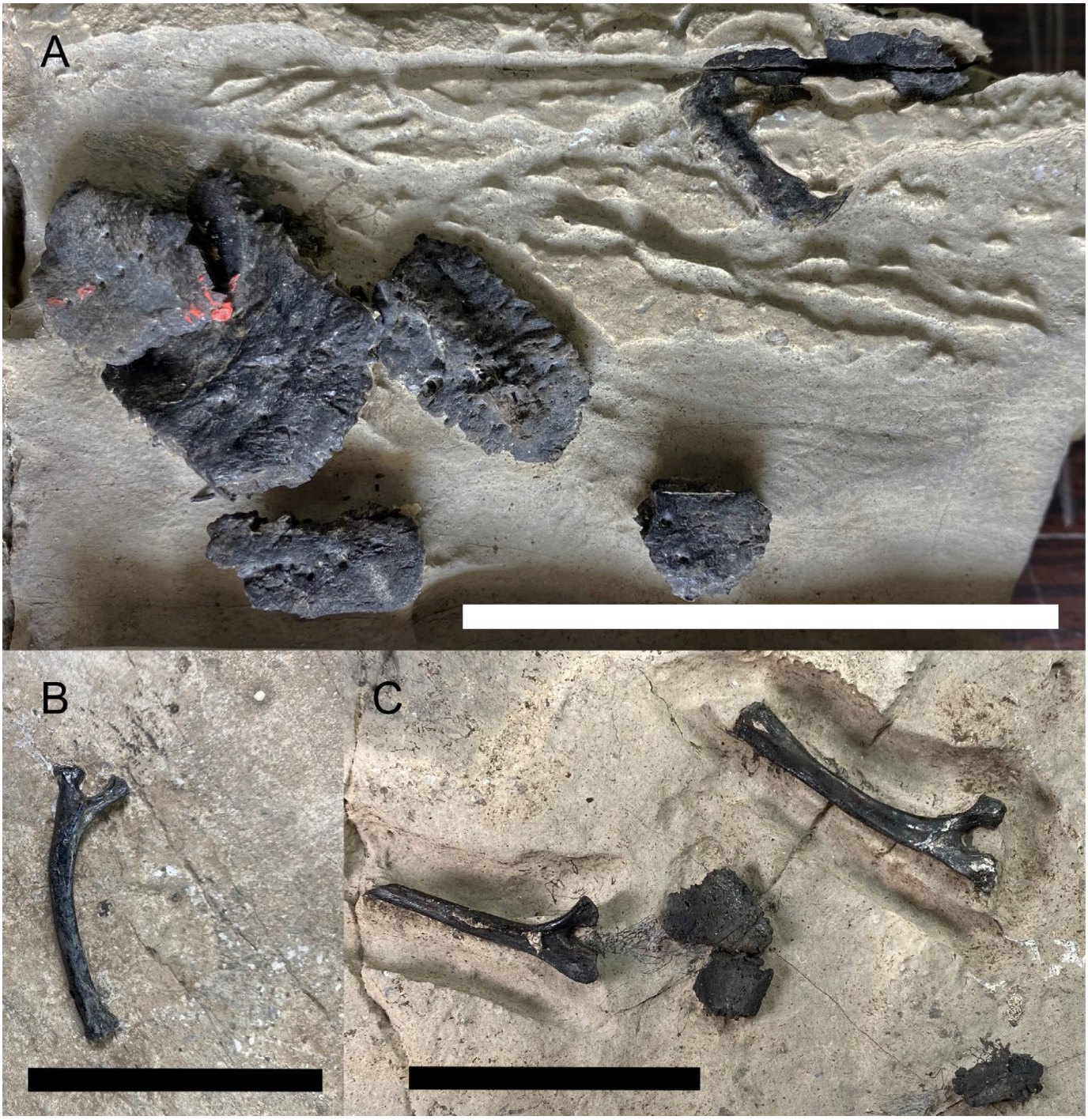

Fig. 2. Isolated or fragmentary specimens referred to *Acynodon adriaticus*. A: MCSNT21.S239-1.0.22 (57248a), B: MCSNT 57245, C: MCSNT21.S239-1.0.22 (57248b). Scale bar: 5 cm.

informal units, the Aurisina formation and the Cretaceous/Palaeogene (K/Pg) bearing Liburnian formation (or by their equivalent synonyms along the adjacent Slovenian units [see Jurkovšek et al., 2016]). From a sedimentological perspective, the site is included in the Aurisina formation and is represented by sharp *facies* variations from open marine, shallow-water limestones to organic-rich rhythmites, which interbed with breccias that accumulated as underwater bodies by subaqueous, density-driven, sedimentary flows. Each identifiable lamina consists of micro-couplets made by a millimetric-thick, dark colored, organic-rich lamina superimposed to a light lamina made of carbonate mud. Given an overall thickness of ~10 m and a thickness of each couplet ranging from 1 to 2.5 cm, the '*laminites*' lens was estimated to represent a time interval of 4–10 kyrs (Arbulla et al., 2006). However, recent surveys at the site have documented how rhythmites and breccia bodies are folded by sin-depositional slumping and deformed by wet-sediment normal faults, thus largely reducing the estimated depositional length to a few kyrs (Chiarenza et al., 2021). Relevant to our comprehension of the genus *Acynodon*, a recent revision of the fossil content of the site has restricted the dating of the fossil

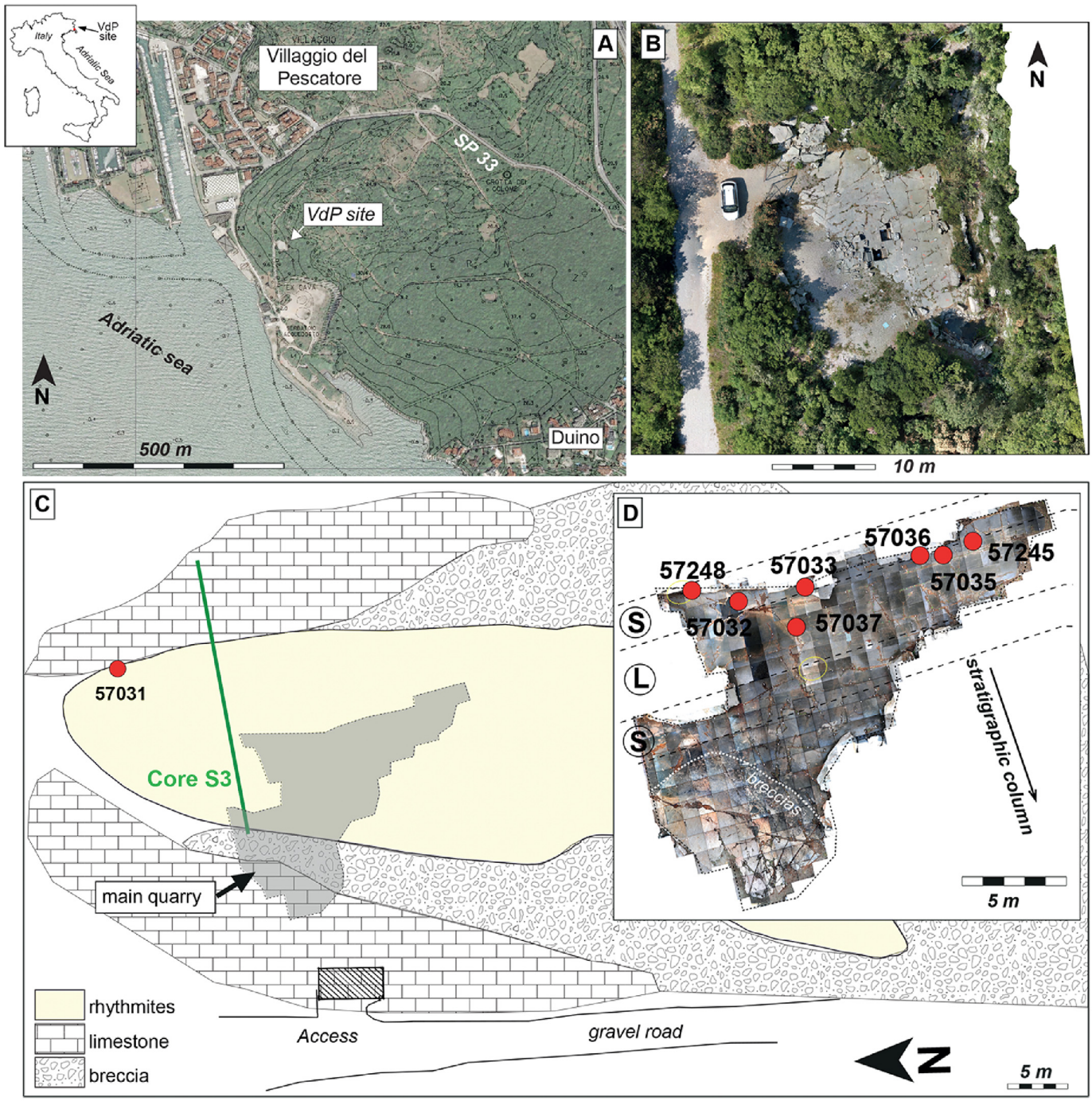

Fig. 3. Geographic and geological setting of the Villaggio del Pescatore quarry. Geographic location of the site (A); ortophotographic view of the quarry obtained with UAV and photogrammetric processing (B), simplified geological map of the site (C) and location of the specimen in the quarry superimposed to GIS-based orthophoto (D). S, slumped rhythmites, L, laminites. Core S3 is the reference core for biostratigraphic analyses (see Chiarenza et al., 2021).

interval to the lower-middle Campanian (81.5–80.5 Ma) based on the vertical distribution of the benthic foraminifera assemblage and calibrated with strontium isotopes stratigraphy (Frijia et al., 2015; Chiarenza et al., 2021). From a stratigraphic perspective, specimen MCSNT 57031 represents the lowermost occurrence of *A. adriaticus* at the site, being collected at the onset of the organic-rich rhythmites. All other elements discussed in this paper are confined in a very restricted interval made of a single, syn-depositional, slumped set of rhythmites. Remarkably, this interval also includes crustaceans, fish, coprolites, and the fully articulated specimens of the hadrosauroid dinosaur *Tethyshadros insularis* (see Chiarenza et al., 2021). Taphonomic and sedimentological parameters support a rapid genetic process for this interval, thus hinting to the presence of a single eusuchian taxon at the site.

3.3. Taphonomy

Slumped rhythmites at the VdP raise crucial questions concerning the taphonomy of the site, including the preservation of vertebrate remains (i.e.: dinosaurs, pterosaurs, crocodiles, fish) in

dysoxic-anoxic bottom waters in marginal-marine settings. Prior to this study, a complete survey of crocodylomorph material from the VdP site was never addressed, and very little was known on the precise stratigraphic occurrence of crocodilian remains within the relatively small fossil-bearing area.

Therefore, for this study, a comprehensive survey of fossil material housed at the MCSNT was undertaken, coupled with a detailed analysis of all available quarry reports and associated photographic material of extractive campaigns between 1996 and 2020 (Dalla Vecchia, 1999; F. Bacchia, pers. comm. 2022). In addition, we used Unmanned Aerial Systems (UAS) and Vehicles (UAV) and related processing technologies to produce the most accurate and up-to-date quarry map (Fig. 3A-C) for the VdP site, a framework into which geological and paleontological data could be precisely included (Fig. 3D). Using these elements we produced an up-to-date list of crocodilian specimens (see 3.1) and were able to relocate each specimen into the stratigraphic setting of the main quarry area. Our data indicate that the occurrence of crocodilian remains is limited to very precise stratigraphic intervals, each represented by a single, slumped, approximately 1.5 m thick, set of laminae (Fig. 3D). These intervals contain the vast majority of fossil remains from the site. Specimen MCSNT 57031 is the lowermost occurrence of crocodilians at the site, found in the proximity of an articulated but poorly preserved individual of *Tethyshadros insularis* (SC 57026). The type specimen of *A. adriaticus* (MCSNT 57248) and most isolated crocodilian elements were collected from the same slump that preserved the type specimen of *T. insularis* (SC 57021) and other nicely preserved and articulated dinosaur remains (SC 57022). Finally, a single isolated bone assigned to an undetermined crocodilian was collected from a third slump in the proximity of a fully articulated skeleton of *T. insularis* (SC 57247) and to other, still *in situ,* articulated dinosaur remains. Remarkably, at the VdP site, large and fully articulated vertebrates are found in association with recurrent fish and crustacean remains: this, coupled with the documented sharp facies variation (open marine limestone to slumped, organic-rich rhythmites interbedded with breccias), rise questions on the depositional processes that led large terrestrial taxa and minute, both freshwater and marine species, to be rapidly buried into anoxic, shallow marine settings.

3.4. Osteohistological sampling

We sampled the 6th dorsal rib and a loose osteoderm fragment (presumably cervical) for osteohistological analyses, in order to investigate the ontogenetic stage of MCSNT 57031. Although long bones have been shown to have a better-preserved growth record, and, therefore, to be more appropriate for quantitative extrapolation of growth strategies and life history, these elements were inaccessible in our sample for curatorial reasons. Furthermore, dorsal ribs and osteoderms have been demonstrated to be excellent skeletal elements for an effective and reliable ontogenetic assessment across tetrapods, and, more specifically, for non-avian archosaurs (Erickson and Brochu, 1999; de Ricqlès et al., 2003, Parker et al., 2008; Scheyer and Sander, 2009; Witzmann, 2009; Witzmann and Soler-Gijón, 2010; Cerda and Desojo, 2011; Scheyer and Desojo, 2011; Woodward Ballard et al., 2011; Taborda et al., 2013; Woodward et al., 2014; Ponce et al., 2017; von Baczko et al., 2019). The thin sections were prepared following the protocol by Chinsamy and Raath (1992), reaching a final thickness of 50–70 microns in the samples that were then analyzed with a Leica DM 2500 P petrographic microscope. Photographs of the thin sections were taken with a ProgRes Cfscan camera. Inference of skeletal maturity follows the recently proposed nomenclature by Griffin et al. (2021).

3.5. Phylogenetic analyses

We scored the holotype of *Acynodon adriaticus* (MCSNT 57248) and MCSNT 57031 as independent Operational Taxonomic Units (OTUs) performing a maximum parsimony and time-calibrated Bayesian phylogenetic analyses. We used the phylogenetic data matrix published by Blanco (2021), an update of the dataset from Narváez et al. (2016) and originally published by Brochu and Storrs (2012). This matrix does not include the Spanish hylaechampsid *Unasuchus* (Brinkmann, 1992), since the limited amount of material referred to the taxon (and the interpretative drawings reported in the literature) allows a minimal amount of scoring in the Blanco's (2021) matrix. Similarly, the Turkish taxon *Turcosuchus* (Jouve et al., 2019) is based on fragmentary material with limited characters scorable in Blanco (2021). A total of 85 out of 189 characters and 31 out of 189 characters were scored for MCSNT 57248 and MCSNT 57031 respectively in Mesquite 3.70 (www.mesquiteproject.org), for a total of 109 OTUs (Data S1).

Characters were treated as unordered and equally weighted. Maximum Parsimony analyses were computed in TNT 1.5 beta (Goloboff et al., 2008), using a 'New Technology' search, with Sect Search, Ratchet, Drift, and Tree Fusing algorithms, and 10 random addition sequences (Chiarenza et al., 2020). A thorough exploration of tree space for obtaining strict consensus and majority rule trees was computed on the trees held in RAM via a 'Traditional Tree Bisection-Reconstruction (TBR) Branch-Swapping' method and both Bootstrap and Bremer support was calculated using standard absolute frequencies for 1000 replicates. The analysis recovered 9 trees with best step length score of 807. Notably, the use of TBR after the 'New Technology' search further explores the tree space (Barrett et al., 2014; Raven and Maidment, 2018). Notably, while this procedure differs from those described in Blanco (2021), Brochu (2011), Narváez et al. (2016) and Puértolas-Pascual et al. (2020), it generated similar general tree topologies, although with different steps and support values.

For the Bayesian analysis, the same nexus file used for the maximum parsimony analyses was expanded following the optimization criteria for 'Morphological Clock Analyses' (Lee et al., 2014) in MrBayes 3.2.7. OTUs' age was matched using midpoint age constraints available in Mannion et al. (2019) and updated following recent chronostratigraphic updates on fossil crocodilian bearing formations (e.g. Chiarenza et al., 2021). Age values and tips in tree were paired using the function 'phylo_check' from the package 'palaeoverse' (Jones et al., 2023) in R version 4.1.3. The MrBayes script encoded the use of a gamma parameter for modeling uniform rate variation across traits, an uncorrelated relaxed clock for modeling rate variation across branches was used instead (igr) of autocorrelated, relaxed clock or a strict clock following Lee et al. (2014). The convergence of all independent runs, together with stationarity were assessed using TRACER v.1.7.1, assuming significance of effective sample size (ESS) for each parameter when $\geq$200 (Rambaut et al., 2018). MrBayes script is included as Data S2. Tree topologies were explored in FigTree v1.4.4. Time-calibrated Bayesian tree was plotted for showing stratigraphic ranges of the tips using the R package 'strap' by Bell and Lloyd (2015), which was also used to calculate values of stratigraphic congruence of different tree outputs compared to randomly generated trees using the Stratigraphic Consistency Index (SCI).

4. Results

4.1. Systematic paleontology

Crocodylomorpha Hay, 1930 *sensu* Nesbitt, 2011
Neosuchia Benton and Clark, 1988

Eusuchia Huxley, 1875 *sensu* Brochu, 2003
Hylaeochampsidae Andrews, 1913
Acynodon Buscalioni et al., 1997

Acynodon adriaticus Delfino et al., 2008a

4.2. Description of MCSNT 57031

Skull

The ventrally exposed cranium (Fig. 4) is roughly 15 cm long, only partially preserved, and obliterated by the slab matrix on its dorsal margin. Based on visible elements (Fig. 4B) it appears to be roughly 80% of the holotype in anteroposterior size (Fig. 5). No maxillary nor premaxillary teeth are visible. Part of the rostral region, although fragmentary, is preserved and corresponds to the palatal portion of the right maxilla (Fig. 4). Very little is preserved of the posterior region of the skull: a wide, subrectangular articular surface (Fig. 4) may represents the ventral portion of the quadrate condyle. However, given the fragmentary preservation, such element may also be the articular glenoid fossa, exposed dorsally due to a rotation of 180°.

The distal section of the right dentary is three-dimensionally preserved, exhibiting clear ornamentations on the labial surface arranged as longitudinal grooves (Fig. 6). The suture with the splenial is located on a deep groove on the ventromedial surface of this distal portion of the mandibular ramus (Fig. 4B). The splenial is well preserved, showing three aligned foramina (Fig. 6). The slab margin is obscured by a protective layer of resin, thus precluding additional observations on the mandible and skull elements. The angular, surangular and articular bones are heavily fragmented and hardly distinguishable. The right retroarticular process is partially damaged but better preserved than the left one, at least in its general outline (Fig. 4). From the posterior end of the retroarticular process to the preserved distal end of the dentary, the right mandibular ramus is 132 mm long and around 10 mm thick dorsoventrally in its distal, less deformed section. The left mandible is represented only by small, hardly identifiable proximal fragments, most likely the angular and articular. One fragment preserves the ornamented surface texture (Fig. 6), with the relatively large pits morphologically similar to those observed on the angular and surangular surfaces of the holotype.

Axial skeleton

The preserved cervical vertebrae are lateroventrally exposed on their left side (Fig. 7): centra show a markedly procoelic condition. Five articulated middle cervical vertebrae, complete with centra, neural arches and cervical ribs are identified and tentatively interpreted as cervicals 3–7, with an anterior neural spine and a few overlapping or nearby fragments corresponding to cervical c2 or c1+c2, and a posteriorly disarticulated tall neural spine probably referable to c8. Given the estimated number of eight total cervical vertebrae in the holotype (Delfino et al., 2008a, 2008b), the series

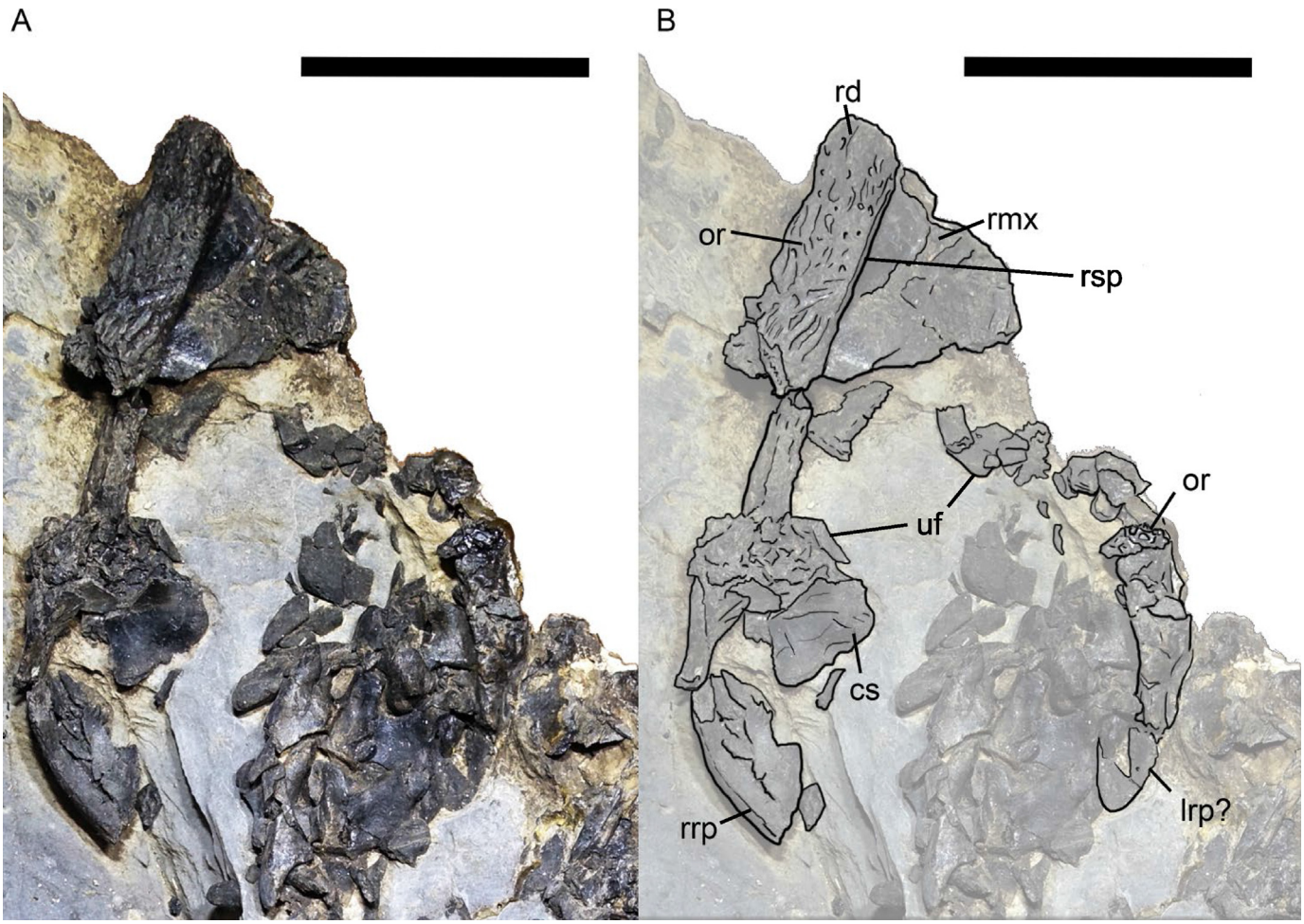

Fig. 4. Skull of MCSNT 57031 (A), with anatomical labels in B. Abbreviations: cs: condylar surface, lrp: left retroarticular process, or: ornamentations, rd: righ dentary, rmx: right maxilla, rrp: right retroarticular process. Scale bar: 5 cm.

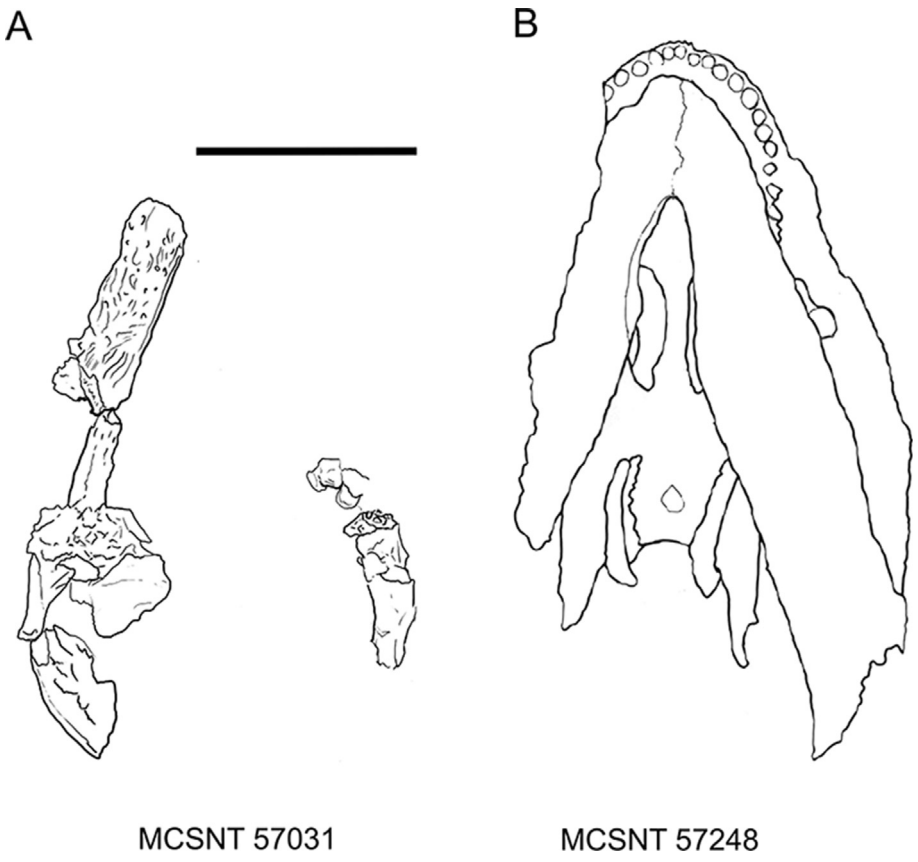

Fig. 5. Cranial outlines in ventral views of specimens referred to *Acynodon adriaticus*, with MCSNT 57031 (A) and the holotype MCSNT 57248 (B). Scale bar: 5 cm.

Fig. 6. Close-up of the dentary of MCSNT 57031 in cranioventral view. d: dentary, f: foramina, sp: splenial. Scale bar: 1 cm.

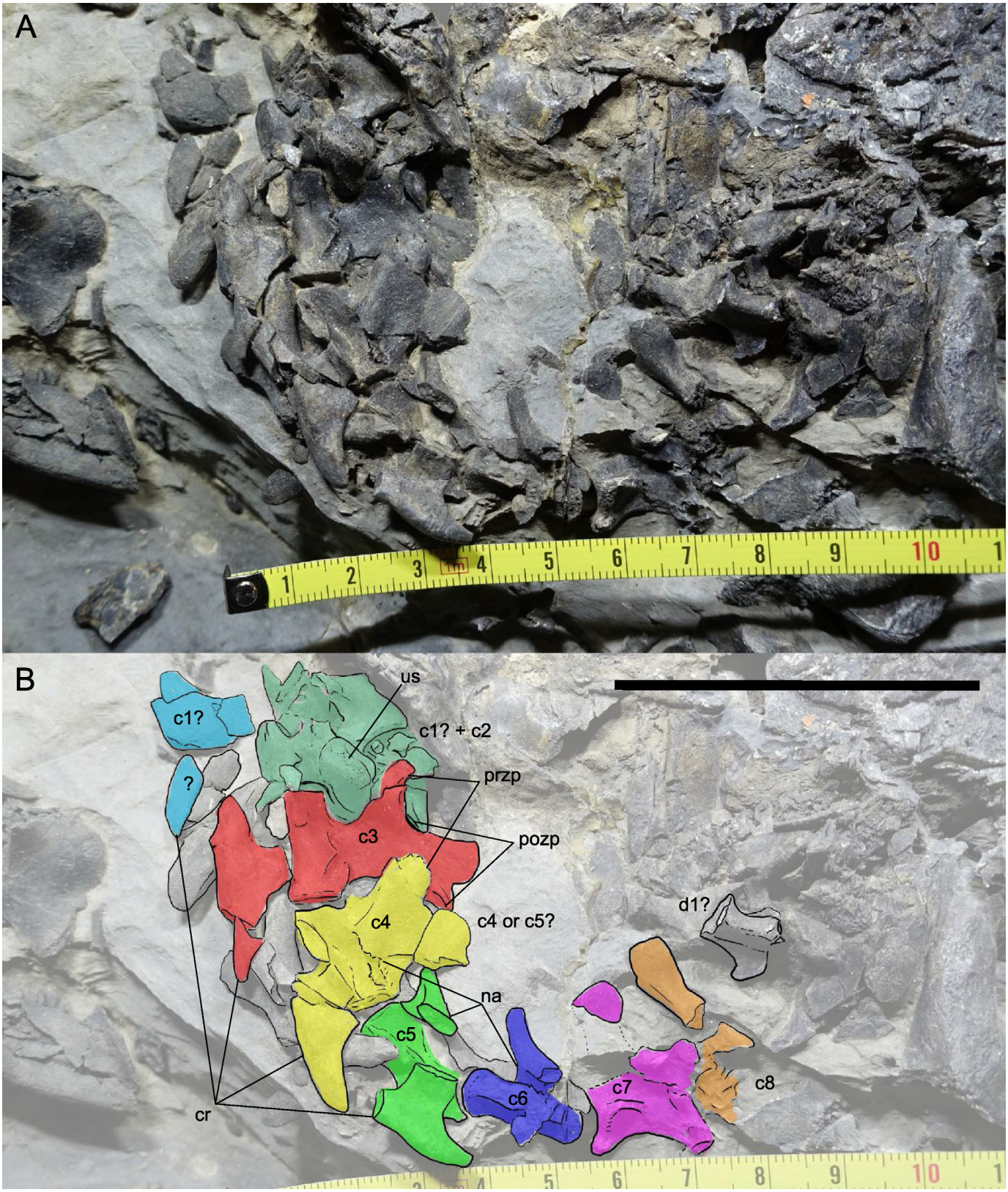

Fig. 7. Cervical series of MCSNT 57031 in lateral view (A) with anatomical labels and outlines highlighted in B. Abbreviations: c: cervical, cr: cervical ribs, d: dorsal, na: neural arch, pozp: postzygapophysis, przp: prezygapophysis, us: unidentified structure. Scale bar: 5 cm.

could be partially overlapped with the holotypic cervical one. Centra are twice anteroposteriorly long as dorsoventrally high. Centra are mediolaterally wide with relatively short and lateroventrally directed parapophyses. The putative c2 centrum is partially lateroventrally rotated, exposing either a convex anterior articular facet, a ventral tuberosity or a blunt hypapophysis. At least 7 cervical ribs are exposed on the surface of the slab, with three well preserved left ribs associated with cervicals 3–5. Ribs have short tubercula and capitula, and they are hatchet-shaped in overall morphology, with a smooth surface and with curved and relatively thick inferior margins. Neural arches are apparently not articulated to each other in cervicals 4–6, and in c5 and c6 they are clearly unfused from their centra, exhibiting open neurocentral sutures (Fig. 7). Both zygapophyses are clearly recognizable in c3, a single c2 postzygapophysis is still articulated to c3 and traces of a prezygapophysis are potentially visible in c4. The c8 neural spine is clearly detached from its arch. Overall, the morphology of the more anterior neural spines is flatter and more anteroposteriorly elongated, gradually becoming proportionally taller and narrower in c5 and c6, with the supposed c8 spine being the tallest of the preserved series, bearing also a distal anteroposterior expansion. An additional vertebral centrum, possibly one of the first dorsal vertebrae, is partially preserved posteriorly to the last cervical neural spine, apparently rotated by almost 180°.

Ribs

Assessing the exact number of preserved ribs is challenging due to the fragmentary nature of the specimen. At least three partial ribs can be recognized on the left side of the animal, located between the bend of the cervical series and the dorsal patch of osteoderms, whereas on the right side, at least nine ribs or partial ribs are preserved (Fig. 8). Their morphology is characterized by a wide anteroposterior expansion along their diaphyses, therefore presumably appearing as a flattened oval shape or eccentrically D-shaped section. The distal epiphysis is preserved in some ribs, appearing to be blunter and more rectangular in their outline in longer posterior ribs than in the anterior ones, consistent with the attachment for cartilage portions connecting the sternal ribs or gastralia. At least three small, elongated structures overlapping with the unidentified clusters of dark bone portions in the abdominal region of the specimen might represent small fragments of gastralia or other sternal ribs (Fig. 8). The dark amorphous mass that partially engulfs them, already described by Delfino et al. (2008b) as a “uniformly vermicular surface”, most likely is here identifiable as a cluster of small lateral or ventral osteoderms exposed on their visceral surface, heavily overlapped and crushed together.

Pectoral girdle

The right coracoid is preserved close to the right humerus and partially overlapped by a narrow-elongated bone, here interpreted as the interclavicle (Fig. 9). The margin of its enlarged distal end appears to be slightly damaged and its proximalmost portion not properly visible. The left coracoid is either not preserved or represented by some fragments located anteriorly to the left humerus. The interclavicle has an enlarged, weakly plate-shaped anterior end. Toward its posterior margin, a short longitudinal keel is visible (Fig. 9). A partially exposed element overlapped by the right coracoid most probably represents the ventrally exposed right scapula. Its shape is consistent with the holotypic right scapula, with subparallel dorsal and ventral margin of the distal portion, but the bad preservation and partial damage in this area prevents a proper description of its morphology at its distalmost process. Given the relevance and direct phylogenetic implication of the scapular blade morphology in crocodilians (see Brochu and Storrs, 2012), we prefer not to define (and score) the morphology of this anatomical trait. The heavily damaged bone between the right scapula and the left humerus can be tentatively referred as the left scapula. The more anterior position of the entire pectoral girdle in the fossil, in relation to the ribs and axial skeleton, suggests an anteriorward slippage of the forelimb-girdle complex from their *in vivo* position.

Right forelimb

Except for a few elements of the manus, the entire right forelimb is exquisitely preserved, although slightly disarticulated. The humerus is ventrally exposed and displays a prominent concave deltopectoral crest with a well-defined apex (Figs. 10, 11), becoming a low longitudinal crest in its proximoventral portion; the deltopectoral crest runs almost up to the distal epiphysis, with a rough apical surface texture reminiscing of a fibrous surface. The proximal epiphysis is not sharply rotated relatively to the distal epiphysis (as described in character 303 by Rio and Mannion, 2021). A relatively large, saddle-like surface lies between the well-developed radial and ulnar condyles, the latter being larger and more laterally prominent. The articular surface of the distal epiphysis exhibits a rough surface, indicating the exact location of the articular cartilage. An interesting detail is the osteoporotic-like bone tissue on the distal condyles (Fig. 12).

The right radius and ulna are robust, medially exposed, parallel to each other (slightly offset from their anatomical position) and near to the distal end of the humerus. They appear to be still articulated at their distal end and only slightly disarticulated proximally. The olecranon process of the ulna is approximately round, the proximal epiphysis is the thickest portion of the bone, the diaphysis gradually becomes thinner towards the distal epiphysis, which is probably missing a small portion, or it is not completely ossified. The radius is distally as thick as the ulna, with a well-developed, wide epiphysis. The epiphyses of both the radius and ulna show a similar osteoporotic bone tissue as in the distal humerus (Fig. 11).

The carpus seems to be complete, and all its elements are lying in anatomical position. The large radiale and ulnare are well preserved with the epiphyseal surfaces showing osteoporotic-like conditions as in the humerus, radius, and ulna (Fig. 12). A carpal element distal to the pisiform seem to be partially fragmented into two separate elements. While the fragmentary nature of these – partially still embedded in matrix – elements prevent a confident identification, one of this may represent the central carpal [centrale *sensu* Gregorovičová et al. (2018); Fig. 12B]. A few bone fragments scattered between the zeugopodium and the carpus may be coming from the anterior proximal portion of the two larger carpals or from the anterior distal end of the radius and/or ulna. The matrix obscures most portions of these elements. Three metacarpals are well preserved, tentatively identifiable as metacarpals I, II and III due to their relative arrangement and position to the carpus. Other two bone elements, possibly the other two metacarpals or phalanges, can be found below these elements. All metacarpals show an even more pronounced epiphyseal bone porosity and irregular surface than every previously mentioned element (Fig. 12). Five phalanges and two closely placed unguals are preserved. The smaller ungual phalanx is found against the metacarpal III, whereas the larger one, relatively big in comparison to the overall forelimb proportions, is characterized by a deep lateral groove, with a short flexor tubercle and pronounced dorsal and ventral process.

In adult crocodylians the carpus has a highly reduced number of ossified elements, with living representatives (e.g. Alligatoridae) having four elements [*Alligator mississippiensis* (Müller and Alberch, 1990), *Caiman yacare* (Lima et al., 2011), *Melanosuchus niger* (Vieira

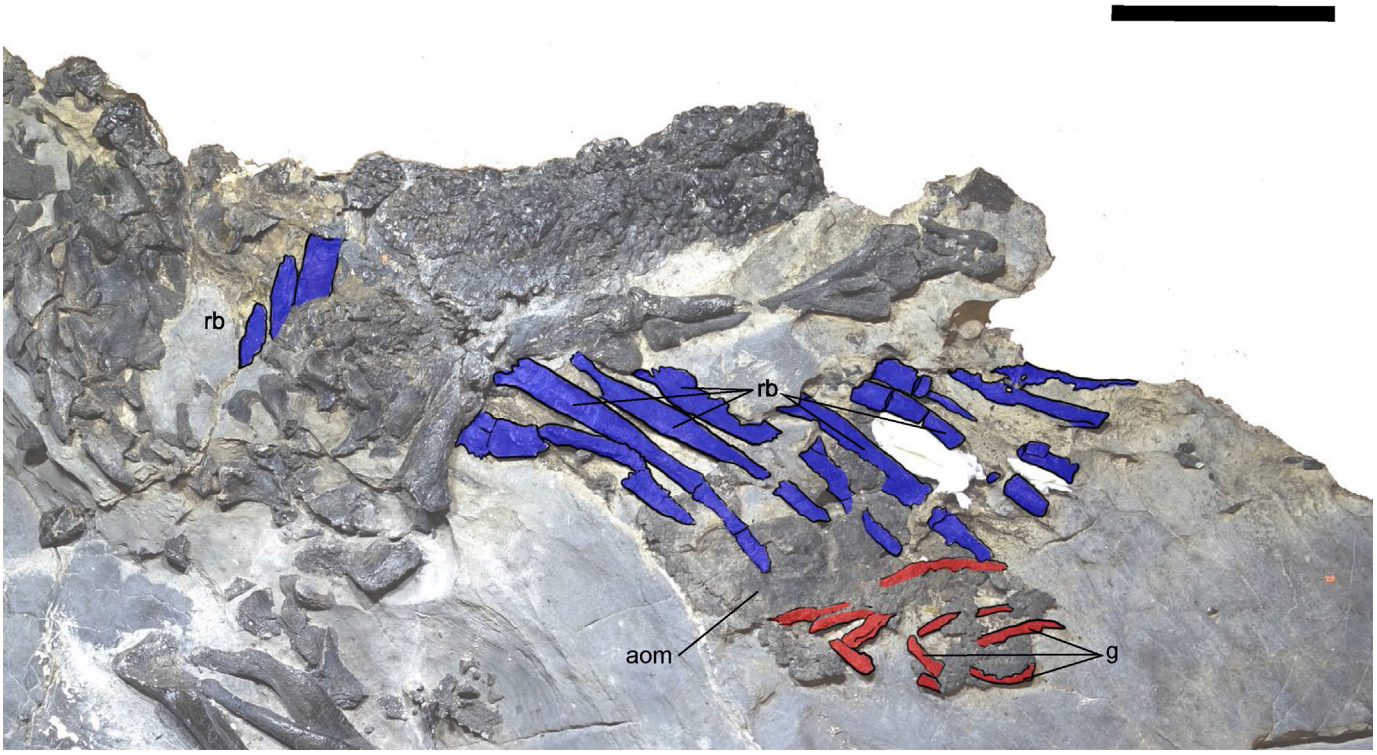

Fig. 8. Ribs of MCSNT 57031 in lateral view with gastralia highlighted in different colors (red) than dorsal ribs (blue). Abbreviations: aom: amorphous osteodermal mass, g: gastralia, rb: ribs. Scale bar: 5 cm.

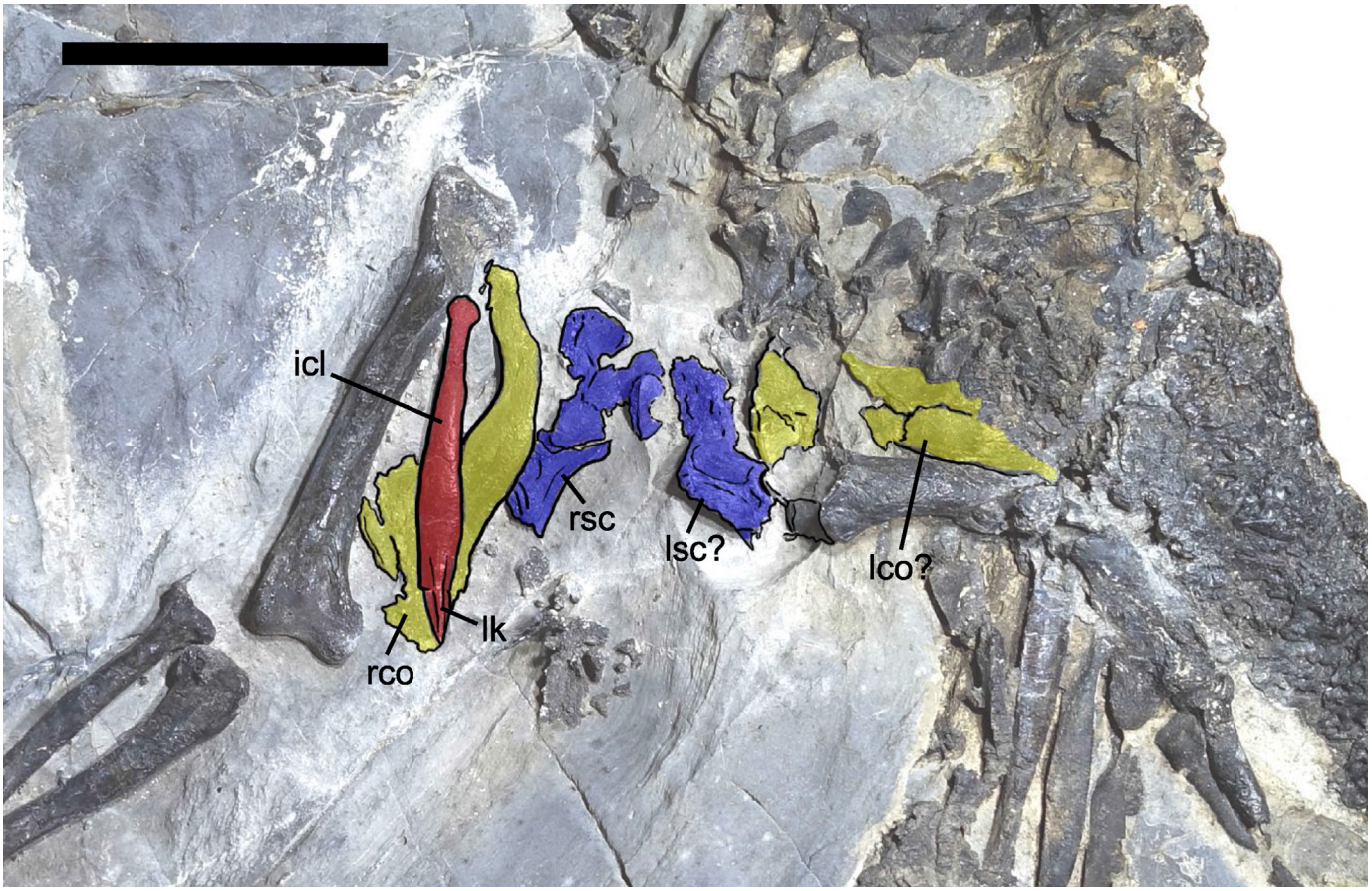

Fig. 9. Pectoral girdle elements of MCSNT 57031 in lateral view. Abbreviations: icl: interclavicle, lco: left coracoid, lk: longitudinal keel, lsc: left scapula, rco: right coracoid, rsc: right scapula. Scale bar: 5 cm.

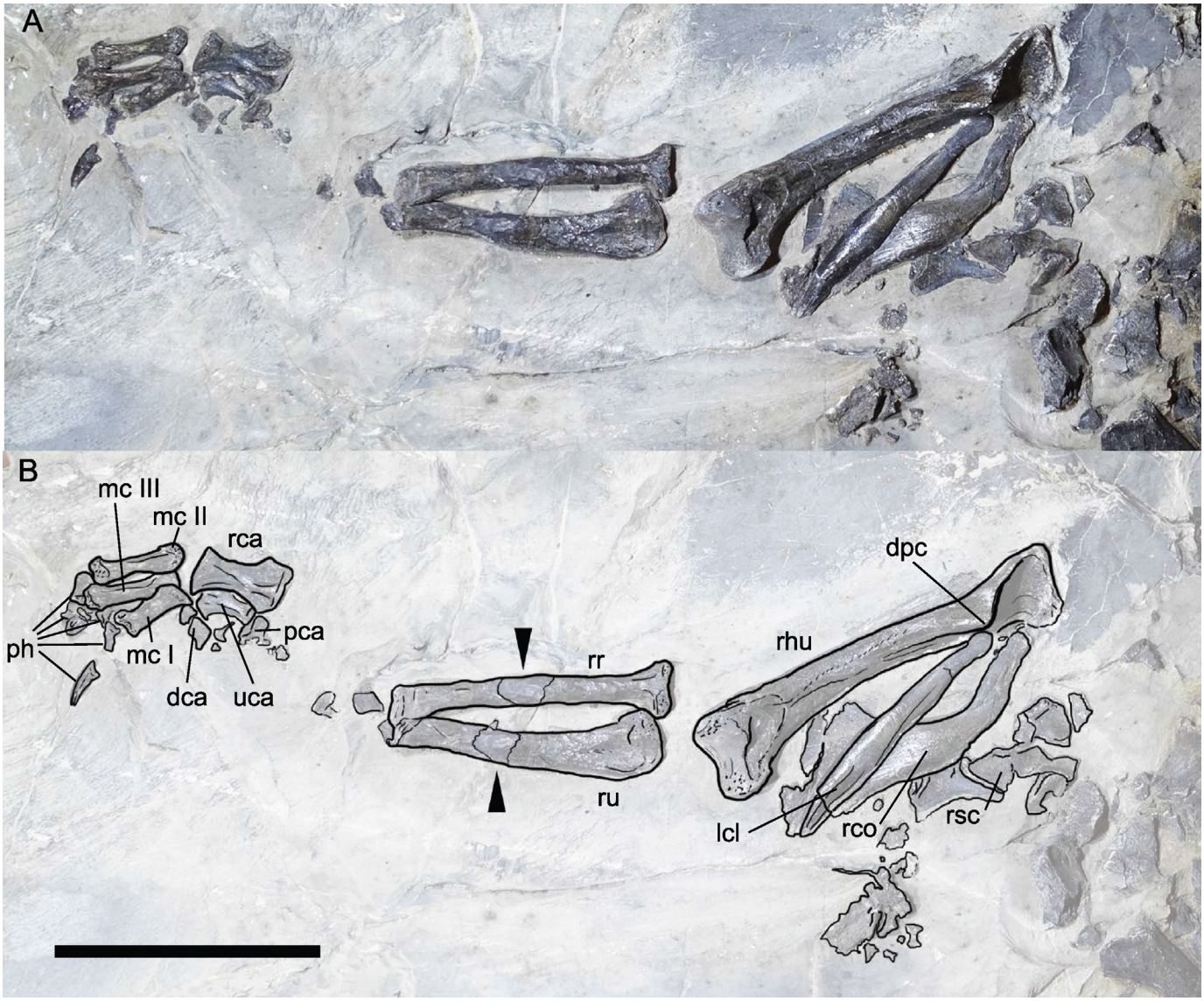

Fig. 10. Right forelimb elements of MCSNT 57031. Arrows indicate restoration in the zeugopodium. Abbreviations: dca: distale carpal, dpc: deltopectoral crest, icl: interclavicle, mc: metacarpal, pca: pisiform carpal, ph: phalanges, rca: radiale carpal, rco: right coracoid, rhu: right humerus, rr: right radius, rsc: right scapula, ru: right ulna, uca: ulnare carpal. Scale bar: 5 cm.

et al., 2018)]. *Acynodon* is therefore expected to reflect a similar condition: in this specimen however, although four major elements are clearly identifiable (Figs. 10, 12), a higher number may be present but obscured by and preservation of these elements.

Left forelimb

Of the left forelimb, the humerus, radius, ulna, the ulnare, and four (possibly five) manual elements are preserved (Fig. 13). The humerus, radius and ulna are badly fragmented, and the bone surface in all of them is not as well preserved as in the right forelimb. The humerus is broken halfway along its proximodistal length. The radius and ulna are overlapping along their proximodistal length and appear broken at their diaphysis. What seems to be a heavily damaged radiale partially overlaps the distal ulnar epiphysis. Up to five other elements are located distally to the radiale including two possible metacarpals or a metacarpal and a carpal. Given their morphology and size, they are here interpreted as an ulnar carpal, two metacarpals and two phalanges (Fig. 13).

Osteoderms

Many osteoderms are preserved in MCSNT 57031 (Fig. 1). A few oval, cervical osteoderms are preserved in ventral view around the cervical area. The largest and most articulated osteoderm cluster is located dorsally to the rib cage. Despite the overall orientation of the specimen (lying on its dorsal side), the entire osteoderm series is dorsally exposed so that the dorsal left rows are visible. Single osteoderms of this area are partially overlapping their neighboring elements on their right and posterior end. This arrangement suggests a 180° rotation of the entire dorsal and lateral osteoderm armor. Ventrally to the anterior elements, however, a smooth surface may in fact represent the somewhat smoother ventral surface of the osteoderms from the row of the right side. Following this interpretation, the whole paravertebral shield would have been affected by a sharp lateral folding along its parasagittal axis. Morphologically, dorsal osteoderms are squared in overall shape, proportionally large mediolaterally and with deep circular pits and grooves surrounded by tall keels on their dorsal surfaces (Fig. 14A). The second anteriormost osteoderm is the best preserved one and

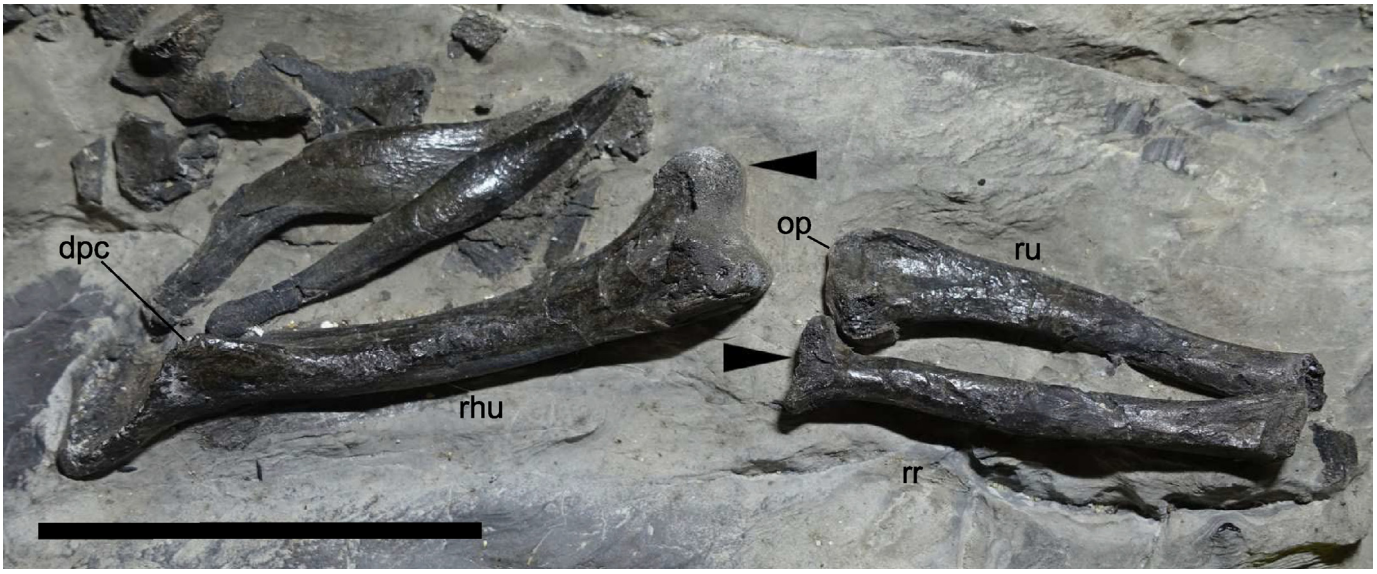

Fig. 11. Details of right forelimb elements of MCSNT 57031. Arrows indicate osteoporotic surfaces. Abbreviations: dpc: deltopectoral crest, op: olecranon process, rhu: right humerus, rr: right radius, ru: right ulna. Scale bar: 5 cm.

displays a radial arrangement of the dorsal ornamentation (Fig. 14B). The majority of other osteoderms exhibit a dorsal tubercular keel running posteriorly and diagonally to the osteoderm quadrangular outline, a feature consistent with the ornamentation of the outer lateral rows of dorsal osteoderms of the paratype MCSNT 57032 described by Delfino et al. (2008a), although they display a much smoother surface. The previously mentioned dark and smooth mass (Fig. 8) located in the abdominal region of the specimen may represent a second cluster of osteoderms. In this roughly polygonal outline, we recognized two main areas: a dorsal one, characterized by a smooth continuous surface, and a ventral amorphous osteoderm mass, with a rougher pattern vaguely reminiscent of black flakes at its margins.

4.3. Osteohistology

Dorsal rib (6th)

The cross section of the dorsal rib appears oval in shape (Fig. 15A). Trabecular bone is present in the medullary cavity, making the transition from the center of the section to the cortex gradual and characterized by intense remodeling (Fig. 15A). The primary bone tissue is composed of lamellar bone (Fig. 15B-C).

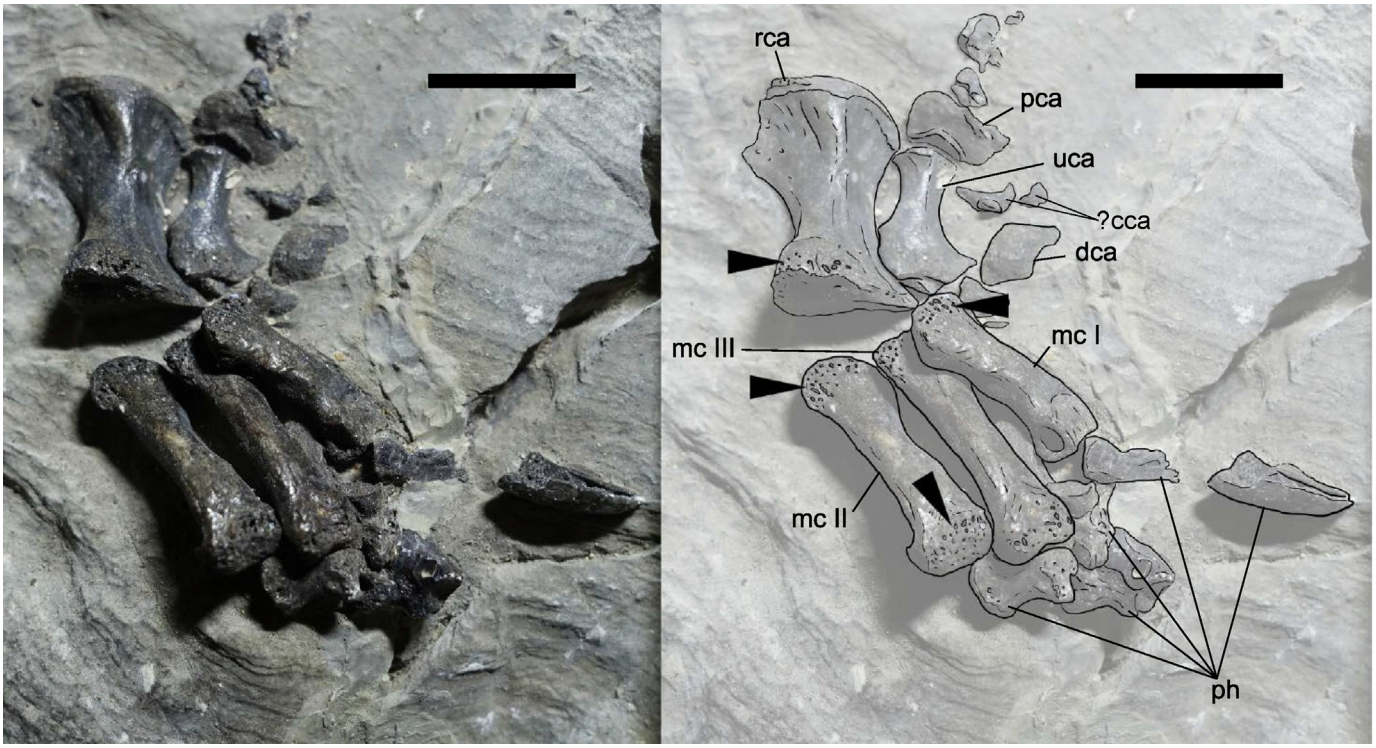

Fig. 12. Details of right autopodium elements of MCSNT 57031. Arrows indicate osteoporotic articular surfaces. Abbreviations: dca: distale carpal, mc: metacarpal, pca: pisiform carpal, ph: phalanges, rca: radiale carpal, uca: ulnare carpal, ?cca, possible fragments of the central carpal (centrale). Scale bar: 1 cm.

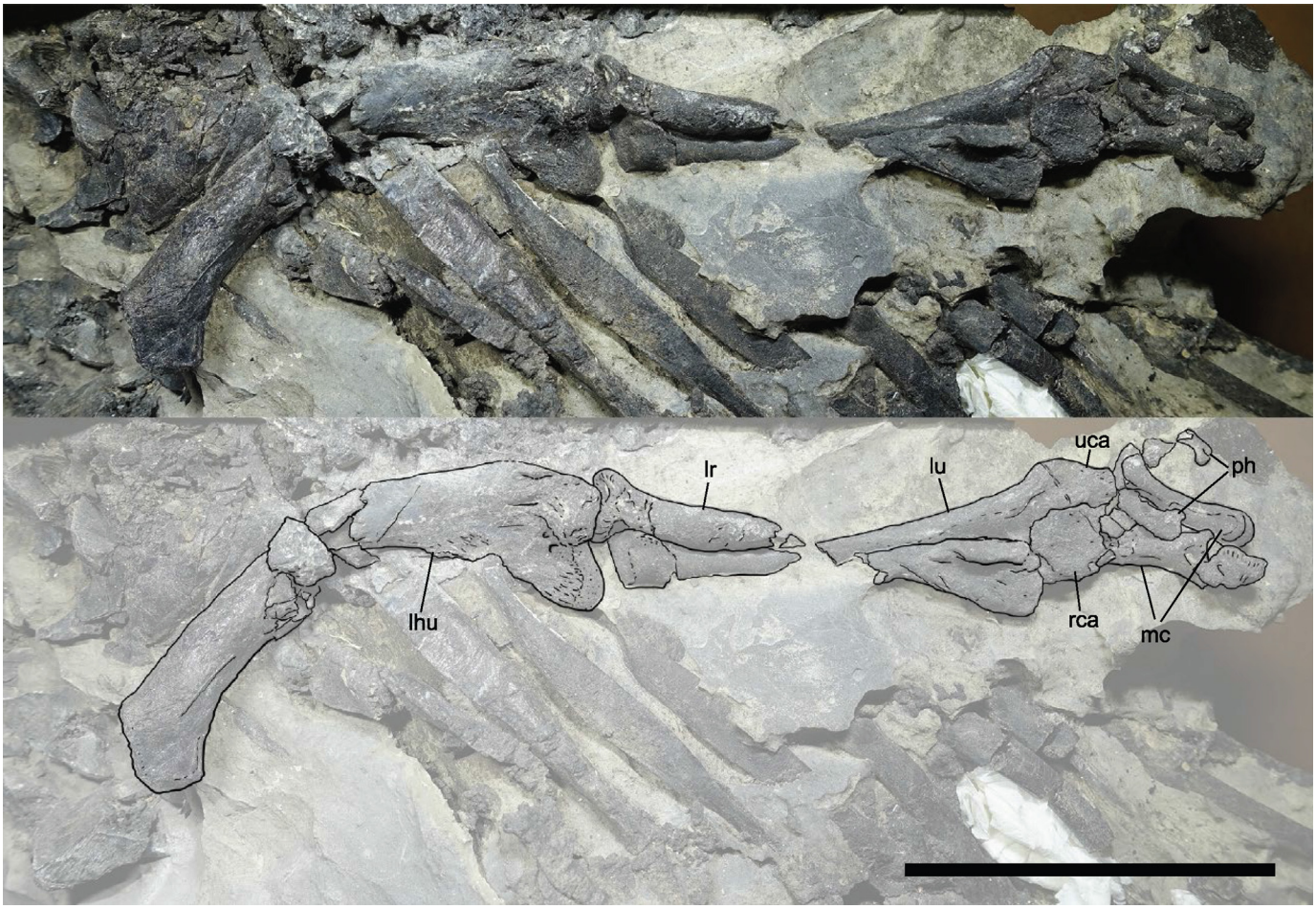

Fig. 13. Left forelimb elements of MCSNT 57031 (A) with anatomical labels reported in B. Abbreviations: lhu: left humerus, lr: left radius, lu: left ulna, mc: metacarpals, ph: phalanges, rca: radiale carpal, uca: ulnare carpal. Scale bar: 5 cm.

Primary vascularization is very rare and sparse, but present, and is mainly longitudinal in orientation. Large, secondary osteons are present in the inner third of the cortex, obscuring the early growth record. 31 Lines of Arrested Growth (LAGs) are present; annuli are commonly present. An External Fundamental System (EFS) is absent.

Osteoderm

The primary bone tissue composing the cortex is constituted by lamellar bone (Fig. 15D-E). Primary vascularization is scarce, but present with a longitudinal orientation. Zonation is present in the preserved primary cortex: 15 LAGs can be counted. Cancellous bone, erosional cavities, and haversian systems obscure the majority of the inner cortex, as generally observed in osteoderms among pseudosuchians. The lower number of LAGs recovered in the cortex of the osteoderm in comparison to the count in the dorsal rib is therefore explained by the overprinting of the early growth record by bone remodeling. An EFS is absent, although zonation tends to decrease and the primary vascularization becomes virtually absent towards the outer surface of the osteoderm.

5. Phylogenetics

The phylogenetic relationships of MCSNT 57031 and the holotype of *A. adriaticus* MCSNT 57248 were tested with maximum parsimony and Bayesian analyses (Fig. 16). The maximum parsimony strict consensus of 9 trees (Fig. 16A, Fig. S2) is 807 steps long, with a Consistency Index of 0.305 and a Retention Index of 0.785. The strict consensus recovers both specimens assigned to *A. adriaticus* in a polytomy with *Hylaeochampsa vectiana* and *Iharkutosuchus makadii* [Bremer (decay) Index of DI = 1]. *Acynodon iberoccitanus* is found as sister group of this polytomy (DI = 2). *Shamosuchus djadochtaensis* and *Pietraroiasuchus ormezzanoi* are found in a polytomy with the *Acynodon* + *Hylaeochampsa* clade (DI = 1). The Majority rule tree (Fig. 16B, Fig. S3) increases resolution in this 'hylaeochampsid polytomy' placing both specimens of *A. adriaticus* (bootstrap support of BS = 77%) as sister group of the clade including *H. vectiana* and *I. makadii* (BS = 100%), but breaking the monophyly of the genus *Acynodon*, since the Spanish eponym taxon *A. iberoccitanus* is found as sister taxon of the *Hylaeochampsa* + *A. adriaticus* clade (BS = 100%). According to this result, a synapomorphy of Hylaeochampsidae is the maxilla with a posterior process between the lacrimal and the prefrontal (character 128, state 2 of Brochu and Storrs, 2012). The synapomorphy defining the *Acynodon* + *Hylaeochampsa* clade is the presence of anterodorsally projected anterior dentary teeth (character 48, state 1 of Brochu and Storrs, 2012). The *Hylaeochampsa* + *A. adriaticus* clade is defined by: a penultimate maxillary alveolus more than twice the diameter of the last maxillary alveolus (character 106, state 1 of Brochu and Storrs, 2012); a prefrontal longer than the lacrimal (character 130, state 1 of Brochu and Storrs, 2012); and a quadrate bearing a prominent, mediolaterally thin crest on its dorsal surface (character 179, state 1 of Brochu and Storrs, 2012). *Acynodon iberoccitanus* is diagnosed in this analysis by the

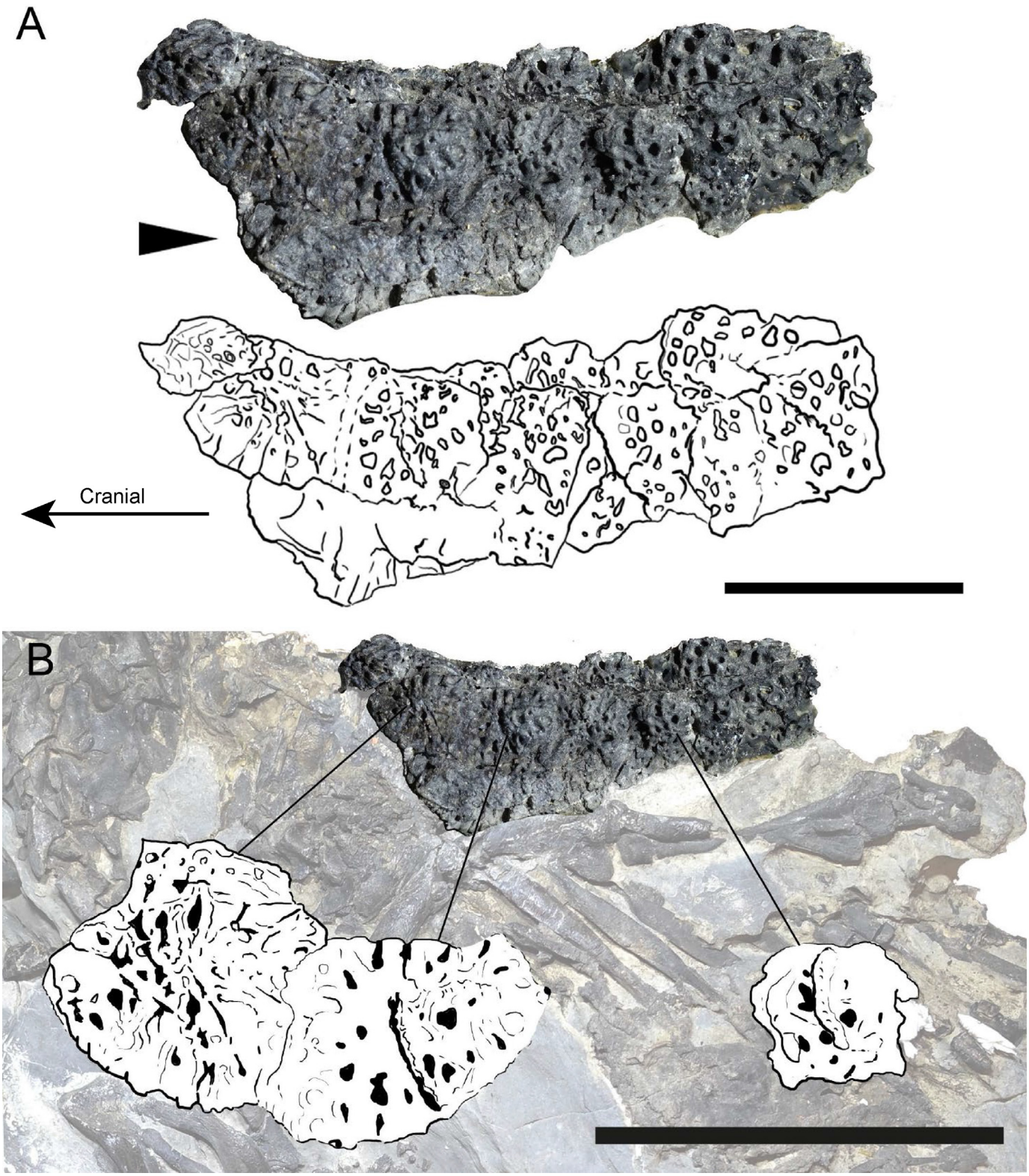

Fig. 14. Osteodermal series of MCSNT 57031 sketched and in different light direction (A) and morphological outlines of the best-preserved ones in B. Black triangle points to possible ventrally exposed osteoderms (see section 4.2). Arrows points to the direction towards the cranium of the specimen. Scale bars: 5 cm.

unexposed supraoccipital on the dorsal surface of the skull table (character 160, state 1 of Brochu and Storrs, 2012).

The Bayesian analysis (Fig. 16C; Fig. S4) solves this paraphyletic ambiguity by placing *A. adriaticus* and *A. iberoccitanus* in a monophyletic clade, with a Posterior Probability (PP) value of 80. The genus *Acynodon* is sister taxon of *I. makadii* (PP = 60), and both form the sister group of *H. vectiana* (PP = 91). This hylaeochampsid clade is sister group (PP = 86) of a lineage including

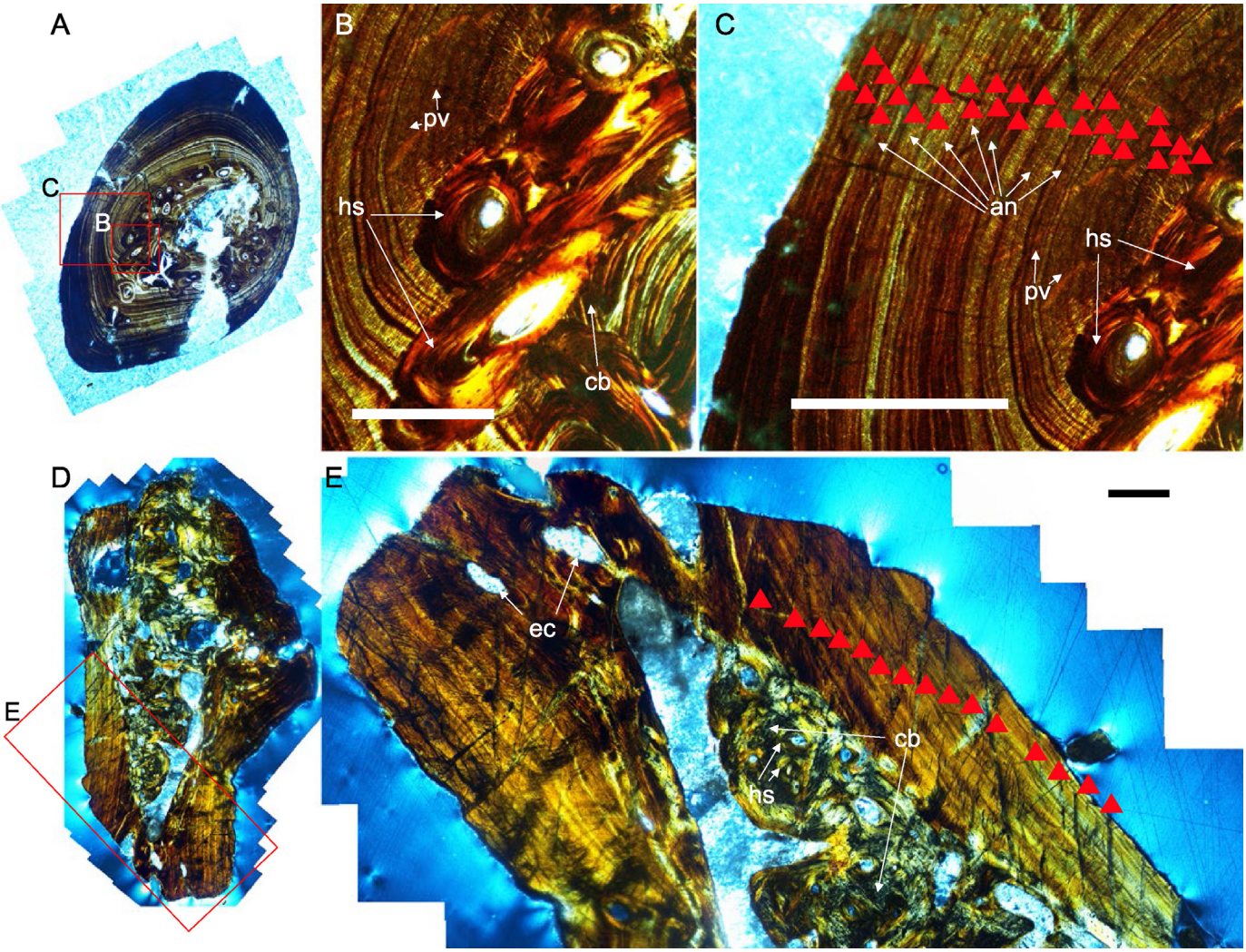

Fig. 15. Histological thin sections under polarized light of MCSNT 57031 6th dorsal rib. A, overall rib histological section; B, detail of secondary osteons, C, lines of arrested growth (LAGs) and annuli in the outer cortex of the rib section; D, overview of the osteoderm thin section; E, close up of the outer cortex of the osteoderm. Scale bars in: B, 250 nm; C, 500 nm; E, 200 nm. Abbreviations: an: annuli; cb: cancellous bone; ec: erosional cavity; hs: haversian system; pv: primary vascularization. Red arrows indicate LAGs.

Pietraroiasuchus ormezzanoi and *Shamosuchus djadochtaensis* (PP = 61). The phylogenetic topology found in the Bayesian analysis has as higher stratigraphic congruence (SCI = 0.5–1 > 0.45; Fig. S5) than the strict consensus (SCI = 0–0.45 > 0.48; Fig. S6) and the majority rule (SCI = 0.5–1 vs 0.585; Fig. S7) trees from the maximum parsimony analysis.

6. Discussion

6.1. Differences between MCSNT 57031 and Acynodon adriaticus holotype MCSNT 57248

Based on overall measurements, MCSNT 57031 is smaller than the holotype MCSNT 57248 (Fig. 17), but single elements show different degree of size disparity between the two specimens. Allometric growth of individual bones is common in crocodilians (Kramer and Medem, 1955; Dodson, 1975; Deeming and Ferguson, 1990), implying that measurements of single bones are inappropriate for precise body size estimations (Brochu, 1996), preventing a further discussion on speculative absolute estimates.

From an overall superimposition between the MCSNT 57031 lower jaw outline and the holotype, some differences emerge (Fig. 5). The holotype possesses a ~20% longer mandible compared to MCSNT 57031, suggesting a larger skull in this individual. The right mandibular ramus of MCSNT 57031 measures 123.4 mm in length, although it is distally incomplete. The maximum mediolateral width of the mandible, when considering from the right angular/surangular region to the highly damaged angular fragments of the left hemimandible, measures 98.5 mm. According to Delfino et al. (2008a, 2008b) the holotype skull is 155 mm long from the distal premaxilla to the posterior edge of the quadrate condyles and is 125 mm wide. Unfortunately, no longitudinal measurements of the ventrally exposed mandibular rami are provided in Delfino et al. (2008a, 2008b), but we provide an overall measurement of 165 mm in length. Although incomplete at the symphyseal region, the holotype mandible is roughly 24% longer than in MCSNT 57031. Intraspecific variability in skull proportions was documented in *Acynodon iberoccitanus* specimens ACAP-FX1 and ACAP-FX2 (Martin, 2007). While considering intraspecific variability a possibility, we consider such differences in available *Acynodon adriaticus* specimens as better explained by taphonomical damage and partial bone dislocation.

As mentioned above, when compared to the holotype, cervical centra in MCSNT 57031 appear proportionally longer and more

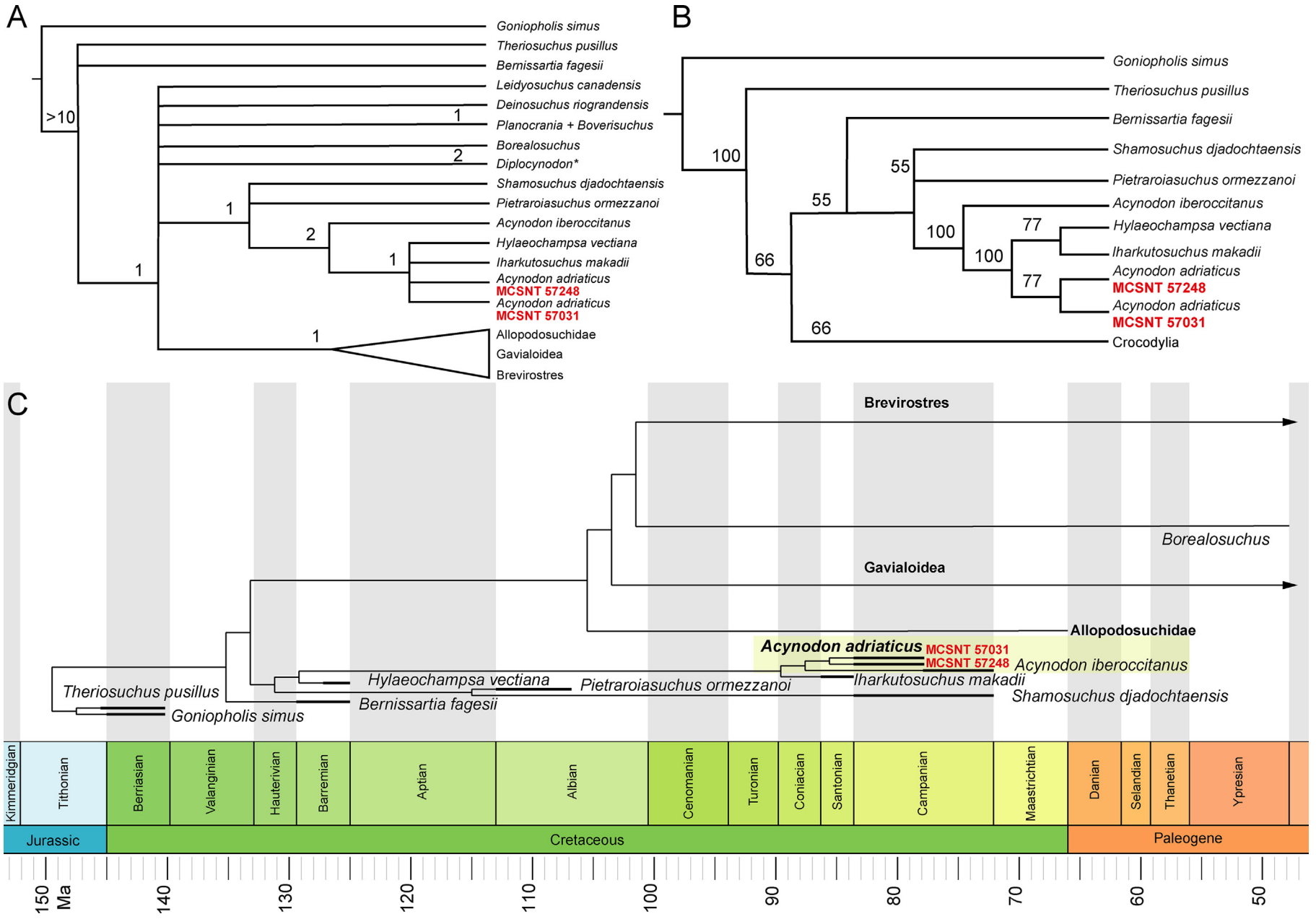

Fig. 16. Phylogenetic position of *Acynodon adriaticus*. Results of maximum parsimony with strict consensus (A) and majority rule (B) trees. Time calibrated Bayesian tree focused on the base of Eusuchia (C). Yellow box is used to highlight the position of the genus *Acynodon*. Specimens referred to *Acynodon adriaticus* highlighted in red. Abbreviation in the chronological y-axis 'Ma' refers to Mega annum (million years). Numbers in A indicate Bremer support (Decay index) while bootstrap support values are reported for the Majority rule tree in B.

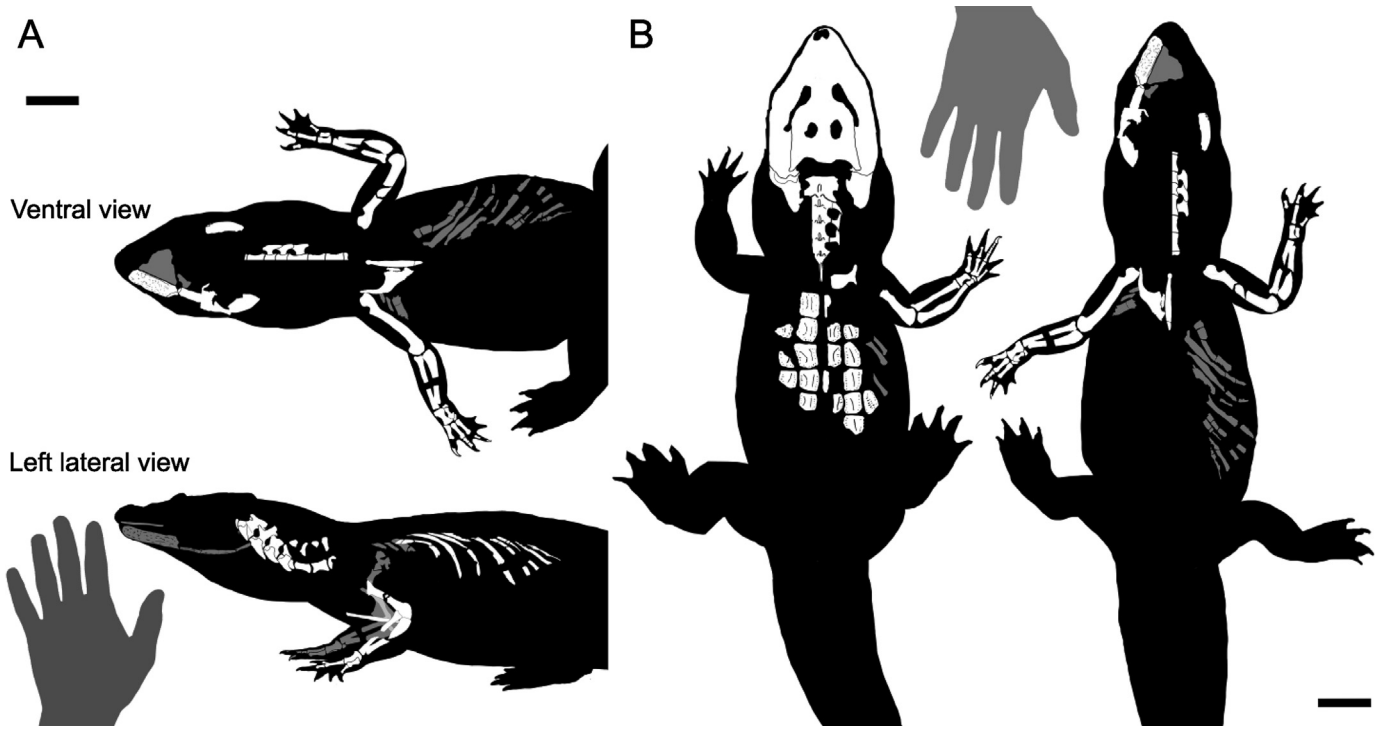

Fig. 17. Skeletal reconstruction of MCSNT 57031 in A with size comparison between the latter specimen in ventral view and the holotype (more complete in dorsal view) in B.

gracile, most likely due to differential preservation. Delfino et al. (2008a, 2008b) estimated an anteroposterior length of 17 mm for the holotypic c6 centrum. We measured the putative c6 centrum in MCSNT 57031 reporting the same measurement (17.2 mm long), thus comparable in anteroposterior length. In the holotype, the neurocentral sutures of all visible vertebrae are closed (Delfino et al., 2008a), suggesting developmental maturity at the time of death (Brochu, 1996). Cervical vertebrae of MCSNT 57031 show detached neural arches from the respective centra along relatively smooth section-like fractures, most probably representing open neurocentral sutures (Fig. 7). Neurocentral sutures in the crocodilian axial skeleton follow a distinct caudal to cranial closure sequence during ontogeny, with the sutures in caudal vertebrae being fully closed in hatchlings, and closure of remaining sutures toward the cranium occurring progressively later. Closure of the cranial-most sutures occurs relatively late in ontogeny and indicates the attainment of morphological maturity (Brochu, 1996). Without histological information, this trait in MCSNT 57031 might be interpreted as a signal of developmental immaturity.

The bone surface on the epiphysis of long bones and manual elements in MCSNT 57031 is consistently osteoporotic, a condition not documented in the holotype. Similar but not identical traits are often linked to skeletal immaturity in tetrapods. This trait however affects a different region of the bone, and Tumarkin-Deratzian et al. (2006) demonstrated that little to no association was present between bone textures and either body size or skeletal maturity in *Alligator mississippiensis*, possibly due to the extremely plastic environment-induced developmental rates common to most crocodilians. This makes the porosities on MCSNT 57031 a weak immaturity signal if considered alone, although it is still widely used for other archosaurs, particularly of the avian lineage (Bennett, 1993; Sampson et al., 1997; Carr, 1999; Chiappe and Göhlich, 2010; Hone et al., 2016; Chiarenza et al., 2020). In contrast, the osteoarthropathy of unknown etiology reported by Huchzermeyer et al. (2013) in *Crocodylus niloticus* is not correlated to ontogenetic immaturity, and the reported humeral epiphyseal osteolytic lesions are somewhat similar to the condition described for MCSNT 57031. The pathological nature of the epiphyseal porosity discussed here should not be excluded.

Although not somatically mature, ontogenetic immaturity (juvenile ontogenetic stage) can be rejected in MCSNT 57031 based on osteohistological results. The amount of remodeling in the inner cortex of the dorsal rib, the high number of LAGs, and the decrease of spacing between them suggest that sexual maturity was probably reached in this individual (Fig. 15). These results contrast with the osteological observations suggesting an immature ontogenetic stage for MCSNT 57031. Although it is currently unclear why such mismatch between these observations is present, previous studies have shown how osteohistological analyses are generally preferable and more reliable than gross osteological observations (e.g. Griffin et al., 2021). Lack of closure for neurocentral sutures along the axial skeleton and porous epiphyses in the long bones have been previously observed in late ontogenetic stages in aquatic animals, such as marine reptiles: these were described as skeletal paedomorphosis and suggested to be an adaptation to more aquatic ecologies (e.g. Rieppel, 1989; Motani et al., 2015). A paedomorphic overall skeletal morphology due to the potentially bizarre ecomorphology of *Acynodon adriaticus* is a possibility, although more data and observations are necessary to confirm this.

6.2. *Phylogenetic implications of MCSNT 57031 for the phylogeny of* Acynodon

Few morphological characters in MCSNT 57031 improved previous scorings of *A. adriaticus* material in the available character matrix. Character 26 in Brochu and Storrs (2012), related to the scapulocoracoid facet anterior to glenoid fossa and previously unscored in the holotype, is scored here from MCSNT 57031 as broad immediately anterior to glenoid fossa, and tapering anteriorly. Similarly, the olecranon process of the ulna (Character 29 in Brochu and Storrs, 2012) is scored as wide and rounded. The

dentary is scored as gently curved in MCSNT 57031 (Character 50 in Brochu and Storrs, 2012), a feature previously unscored from the holotype. The strict consensus from maximum parsimony analysis recovers a complete polyotomy of the main groups of Eusuchia when the specimen MCSNT 57031 is added to the dataset, whereas when this OTU is inactive, the topology between the main eusuchian lineages is identical to that reported by Blanco (2021). This is probably due to the low proportion of diagnosable characters in this specimen of *A. adriaticus*.

On a purely morphological basis and under a maximum parsimony approach, the phylogenetic integration of the new scoring confirms the paraphyly of *Acynodon* as shown in several previous analyses (Brochu, 2011; Brochu, 2012; Brochu et al., 2012; Martin et al., 2014, 2016; Narváez et al., 2016; Jouve et al., 2019; Ristevski et al., 2020; Blanco, 2021). If confirmed, this may require the erection of a new genus, based exclusively on the material from VdP, but further reconsideration including a redescription of the other species included in *Acynodon*, at the light of several newly described characters of phylogenetic value, is strongly needed. In particular, a better scoring of the poorly preserved hylaeochampsids and the retrieval of new remains (above all *Hylaeochampsa*) would be also recommended in order to properly revaluate the phylogeny and therefore taxonomy of *Acynodon* as well as the phylogenetic position of Hylaeochampsidae and closely related taxa within Eusuchia.

We remark that the chronostratigraphic re-evaluation of the age of VdP to the early–middle Campanian improves stratigraphic congruence and sets the specimens of *A. adriaticus* as chronologically older and stratigraphically overlaid by the biostratigraphic range of *A. iberoccitanus*. Furthermore, the Bayesian analysis re-establishes the monophyly of *Acynodon*, creating ambiguity between parsimony-based and Bayesian-based topologies. These results shorten the ghost lineage between *Hylaeochampsa* and *A. iberoccitanus* resulting from previous tip-dated Bayesian analyses of crocodylomorph taxa (Lee and Yates, 2018). The question of the monophyly of *Acynodon* is probably key to solve the relationships between hylaeochampsids and may bear some weight on the resolution of this clade inside Eusuchia (and early diverging eusuchian relationships overall). The morphological redescription and chronostratigraphic datum added herein are preliminary steps to increase the resolution at the base of Eusuchia and provide a better understanding of the palaeobiology and evolutionary history of this interesting clade of Mesozoic crocodylomorphs from the Tethyan domain.

7. Conclusions

A detailed description of specimen MCSNT 57031 herein referred to *Acynodon adriaticus* offers a new opportunity to evaluate the variation in the fossil eusuchians from Villaggio del Pescatore locality. The latest Cretaceous genus *Acynodon* is herein found monophyletic by the Bayesian analysis, with the Italian taxon representing an earlier diverging species from the lower-middle Campanian while the eponym taxon *Acynodon iberoccitanus* occupies a more recent chronostratigraphic range (middle-late Campanian). The Parsimony-based phylogenetic results, though, is in conflict with this interpretation, creating a paraphyletic *Acynodon*, probably also induced by the poorly phylogenetically sampled sister taxa (e.g. *Hylaeochampsa*), for which a redescription and more complete phylogenetic scoring would be recommended (ideally, supplemented by new and more complete material). We highlight the need for a detailed and descriptive phylogenetic work focusing on key taxa at the base of Eusuchia, to resolve the phylogenetic relationships of these taxa (i.e. 'hylaeochampsids') and resolve the taxonomy of *Acynodon*, with important possible repercussions on the palaeobiology of these remarkable peri-Tethyan crocodylomorphs, highlighted by the interesting asynchrony between histological and morphological maturity-related traits in its skeleton.

Data availability

All data discussed in the paper are included as figures, tables or in the Supplementary material.

Acknowledgments

The authors thank all those involved in this research project on the Villaggio del Pescatore site: we hope scientific results will once again remark the uniqueness of this paleontological site and promote its protection and promotion by all institutional offices. The Soprintendenza Archeologia, Belle Arti e Paesaggio del Friuli Venezia Giulia facilitated the study of the vertebrate remains from the Villaggio del Pescatore (prot. 3289 dd. 22/02/2022 to F. Fanti). We wish to thank S. Bonomi and P. Ventura (SABAP) for their commitment to scientific research related to the Villaggio del Pescatore site. We thank P. Fasolato, F. Locci, D. Arbulla and the staff of the Museo Civico di Storia Naturale in Trieste for granting access to VdP material in their care. This work greatly benefited from the comments by the Editor E. Koutsoukos, A. Blanco and an anonymous reviewer. Discussions with L. Cantelli (UniBo) and L. Consorti (CNR-ISMAR) improved this manuscript. We are indebted with F. Bacchia and G. Bacchia (Zoic s.r.l.) for disclosing personal and historical information on the site. We also thank M. Sartori, F. Gamberini, and the Comune di Duino Aurisina. We acknowledge that images of specimens provided in this study are curtesy of Soprintendenza ABAP FVG -MiC (art. 108, co.3 D. Lgs 42/2004 s.m.i). A.A.C. was supported through the European Research Council (ERC) starting grant under the European Union's Horizon 2020 research and innovation program, grant agreement no. 947921, MAPAS at the Universidade de Vigo (Spain) and by a Juan de la Cierva-formación 2020 fellowship funded by FJC2020-044836-I/MCIN/AEI/10.13039/501100011033 by the European Union "NextGenerationEU"/PRTR.

References

Andrews, C.W., 1913. LVIII.—On the skull and part of the skeleton of a crocodile from the Middle Purbeck of Swanage, with a description of a new species (*Pholidosaurus lævis*), and a note on the skull of Hylæochampsa. Annals and Magazine of Natural History 11, 485–494. https://doi.org/10.1080/00222931308693345.

Arbulla, D., Cotza, F., Cucchi, F., Dalla Vecchia, F.M., De Giusto, A., Flora, O., Masetti, D., Palci, A., Pittau, P., Pugliese, N., Stenni, B., Tarlao, A., Tunis, G., Zini, L., 2006. La successione Santoniano–Campaniana del Villaggio del Pescatore (Carso Triestino) nel quale sono stati rinvenuti i resti di dinosauro. In: Guida Alle Escursioni/Excursions Guide, Società Paleontologica Italiana. Presented at the Giornate di Paleontologia 2006. EUT Edizioni Università di Trieste, Trieste, pp. 20–27.

Attura, M., 1999. Aspetti paleontologici e geochimico-isotopici di una successione stratigrafica Santoniana-Camapaniana del Villaggio del Pescatore (Ts). Università degli Studi di Trieste, Trieste.

Barrett, P.M., Butler, R.J., Mundil, R., Scheyer, T.M., Irmis, R.B., Sánchez-Villagra, M.R., 2014. A palaeoequatorial ornithischian and new constraints on early dinosaur diversification. Proceedings of the Royal Society B: Biological Sciences 281, 20141147. https://doi.org/10.1098/rspb.2014.1147.

Bell, M.A., Lloyd, G.T., 2015. strap: an R package for plotting phylogenies against stratigraphy and assessing their stratigraphic congruence. Palaeontology 58, 379–389. https://doi.org/10.1111/pala.12142.

Bennett, S.C., 1993. The ontogeny of *Pteranodon* and other pterosaurs. Paleobiology 19, 92–106.

Benton, M.J., Clark, J.M., 1988. Archosaur phylogeny and the relationships of the Crocodylia. Environmental Science 295–338.

Blanco, A., 2021. Importance of the postcranial skeleton in eusuchian phylogeny: Reassessing the systematics of allodaposuchid crocodylians. PLoS One 16, e0251900. https://doi.org/10.1371/journal.pone.0251900.

Blanco, A., Puértolas-Pascual, E., Marmi, J., Moncunill-Solé, B., Llácer, S., Rössner, G.E., 2020. Late Cretaceous (Maastrichtian) crocodyliforms from north-

eastern Iberia: a first attempt to explain the crocodyliform diversity based on tooth qualitative traits. Zoological Journal of the Linnean Society 189, 584–617. https://doi.org/10.1093/zoolinnean/zlz106.
Brinkmann, W., 1992. Die Krokodilier-Fauna aus der Unter-Kreide (Ober-Barremium) von Una (Provinz Cuenca, Spanien). Herausgegeben von geowissenschaftlichen Instituten der Freien und der Technischen. Universität Berlin und der Technischen Fachhochschule, Berlin.
Brochu, C.A., 1996. Closure of neurocentral sutures during crocodilian ontogeny: Implications for maturity assessment in fossil archosaurs. Journal of Vertebrate Paleontology 16, 49–62. https://doi.org/10.1080/02724634.1996.10011283.
Brochu, C.A., 1999. Phylogenetics, taxonomy, and historical biogeography of Alligatoroidea. Journal of Vertebrate Paleontology 19, 9–100. https://doi.org/10.1080/02724634.1999.10011201.
Brochu, C.A., 2001. Crocodylian snouts in space and time: phylogenetic approaches toward adaptive radiation. American Zoologist 41, 564–585. https://doi.org/10.1093/icb/41.3.564.
Brochu, C.A., 2003. Phylogenetic Approaches Toward Crocodylian History. Annual Review of Earth and Planetary Sciences 31, 357–397. https://doi.org/10.1146/annurev.earth.31.100901.141308.
Brochu, C.A., 2010. A new alligatorid from the lower Eocene Green River Formation of Wyoming and the origin of caimans. Journal of Vertebrate Paleontology 30, 1109–1126. https://doi.org/10.1080/02724634.2010.483569.
Brochu, C.A., 2011. Phylogenetic relationships of *Necrosuchus ionensis* Simpson, 1937 and the early history of caimanines. Zoological Journal of the Linnean Society 163, S228–S256. https://doi.org/10.1111/j.1096-3642.2011.00716.x.
Brochu, C.A., 2012. Phylogenetic relationships of Palaeogene ziphodont eusuchians and the status of *Pristichampsus* Gervais, 1853. Earth and Environmental Science Transactions of The Royal Society of Edinburgh 103, 521–550. https://doi.org/10.1017/S1755691013000200.
Brochu, C.A., Parris, D.C., Grandstaff, B.S., Denton, R.K., Gallagher, W.B., 2012. A new species of *Borealosuchus* (Crocodyliformes, Eusuchia) from the Late Cretaceous–early Paleogene of New Jersey. Null 32, 105–116. https://doi.org/10.1080/02724634.2012.633585.
Brochu, C.A., Storrs, G.W., 2012. A giant crocodile from the Plio-Pleistocene of Kenya, the phylogenetic relationships of Neogene African crocodylines, and the antiquity of Crocodylus in Africa. Journal of Vertebrate Paleontology 32, 587–602. https://doi.org/10.1080/02724634.2012.652324.
Buscalioni, A.D., Ortega, F., Vasse, D., 1997. New crocodiles (Eusuchia: Alligatoroidea) from the Upper Cretaceous of southern Europe. Comptes Rendus de l'Academie des Sciences – Series IIA: Earth and Planetary Science 325, 525–530. https://doi.org/10.1016/S1251-8050(97)89872-2.
Carr, T.D., 1999. Craniofacial ontogeny in tyrannosauridae (Dinosauria, Coelurosauria). Journal of Vertebrate Paleontology 19, 497–520.
Cerda, I.A., Desojo, J.B., 2011. Dermal armour histology of aetosaurs (Archosauria: Pseudosuchia), from the Upper Triassic of Argentina and Brazil. Lethaia 44, 417–428. https://doi.org/10.1111/j.1502-3931.2010.00252.x.
Chiappe, L.M., Göhlich, U.B., 2010. Anatomy of *Juravenator starki* (Theropoda: Coelurosauria) from the late Jurassic of Germany. Neues Jahrbuch fuer Geologie und Palaeontologie Abhandlungen 258, 257–296.
Chiarenza, A.A., Fiorillo, A.R., Tykoski, R.S., McCarthy, P.J., Flaig, P.P., Contreras, D.L., 2020. The first juvenile dromaeosaurid (Dinosauria: Theropoda) from Arctic Alaska. PLoS One 15, e0235078. https://doi.org/10.1371/journal.pone.0235078.
Chiarenza, A.A., Fabbri, M., Consorti, L., Muscioni, M., Evans, D.C., Cantalapiedra, J.L., Fanti, F., 2021. An Italian dinosaur Lagerstätte reveals the tempo and mode of hadrosauriform body size evolution. Scientific Reports 11, 23295. https://doi.org/10.1038/s41598-021-02490-x.
Chinsamy, A., Raath, M.A., 1992. Preparation of fossil bone for histological examination.
Consorti, L., Arbulla, D., Bonini, L., Fabbi, S., Fanti, F., Franceschi, M., Frijia, G., Pini, G.A., 2021. The Mesozoic palaeoenvironmental richness of the Trieste Karst. GFT&M. https://doi.org/10.3301/GFT.2021.06.
Dalla Vecchia, F.M., 1999. Relazione scientifica finale, scavo paleontologico del Villaggio del Pescatore 1998–1999 & elencazione, identificazione e determinazione preliminare dei reperti.
Dalla Vecchia, F.M., 2008. I dinosauri del Villaggio del Pescatore (Trieste): qualche aggiornamento. Atti del Museo Civico di Storia Naturale di Trieste 53, 111–113.
Dalla Vecchia, F.M., 2009. *Tethyshadros insularis*, a new hadrosauroid dinosaur (Ornithischia) from the Upper Cretaceous of Italy. Journal of Vertebrate Paleontology 29, 1100–1116. https://doi.org/10.1671/039.029.0428.
de Ricqlès, A.J., Padian, K., Horner, J.R., 2003. On the bone histology of some Triassic pseudosuchian archosaurs and related taxa. Annales de Paléontologie 89, 67–101. https://doi.org/10.1016/S0753-3969(03)00005-3.
Deeming, D.C., Ferguson, M.W.J., 1990. Morphometric analysis of embryonic development in *Alligator mississippiensis, Crocodylus johnstoni* and *Crocodylus porosus*. Journal of Zoology 221, 419–439. https://doi.org/10.1111/j.1469-7998.1990.tb04011.x.
Delfino, M., Buffetaut, E., 2006. In: Fonda, G., Melis, R., Romano, R. (Eds.), Giornate di Paleontologia della Società Paleontologica Italiana abstracts. Trieste, Italy, 87 pp.
Delfino, M., Martin, J.E., Buffetaut, E., 2008a. A new species of *Acynodon* (Crocodylia) from the upper cretaceous (Santonian–Campanian) of Villaggio del Pescatore, Italy. Palaeontology 51, 1091–1106. https://doi.org/10.1111/j.1475-4983.2008.00800.x.
Delfino, M., Martin, J.E., Buffetaut, E., 2008b. I coccodrilli del Villaggio del Pescatore: una panoramica generale. Atti del Museo Civico di Storia Naturale di Trieste 53, 277–284. .
Dodson, P., 1975. Taxonomic implications of relative growth in Lambeosaurine Hadrosaurs. Systematic Zoology 24, 37–54. https://doi.org/10.2307/2412696.
Erickson, G.M., Brochu, C.A., 1999. How the 'terror crocodile' grew so big. Nature 398, 205–206. https://doi.org/10.1038/18343.
Frijia, G., Parente, M., Di Lucia, M., Mutti, M., 2015. Carbon and strontium isotope stratigraphy of the Upper Cretaceous (Cenomanian-Campanian) shallow-water carbonates of southern Italy: Chronostratigraphic calibration of larger foraminifera biostratigraphy. Cretaceous Research 53, 110–139. https://doi.org/10.1016/j.cretres.2014.11.002.
Goloboff, P.A., Farris, J.S., Nixon, K.C., 2008. TNT, a free program for phylogenetic analysis. Cladistics 24, 774–786. https://doi.org/10.1111/j.1096-0031.2008.00217.x.
Gregorovičová, M., Kvasilová, A., Sedmera, D., 2018. Ossification pattern in forelimbs of the Siamese crocodile (*Crocodylus siamensis*): similarity in ontogeny of carpus among crocodylian species. The Anatomical Record 301, 1159–1168. https://doi.org/10.1002/ar.23792.
Griffin, C.T., Stocker, M.R., Colleary, C., Stefanic, C.M., Lessner, E.J., Riegler, M., Formoso, K., Koeller, K., Nesbitt, S.J., 2021. Assessing ontogenetic maturity in extinct saurian reptiles. Biological Reviews 96, 470–525. https://doi.org/10.1111/brv.12666.
Hone, D.W.E., Farke, A.A., Wedel, M.J., 2016. Ontogeny and the fossil record: what, if anything, is an adult dinosaur? Biology Letters 12, 20150947. https://doi.org/10.1098/rsbl.2015.0947.
Huchzermeyer, F.W., Groenewald, H.B., Myburgh, J.G., Steyl, J.C.A., Crole, M.R., 2013. Osteoarthropathy of unknown aetiology in the long bones of farmed and wild Nile crocodiles (*Crocodylus niloticus*). Journal of the South African Veterinary Association 84, 1–5.
Jones, L.A., Gearty, W., Allen, B.J., Eichenseer, K., Dean, C.D., Galván, S., Kouvari, M., Godoy, P.L., Nicholl, C.S.C., Buffan, L., Dillon, E.M., Flannery-Sutherland, J.T., Chiarenza, A.A., 2023. Palaeoverse: A community-driven R package to support palaeobiological analysis. Methods in Ecology and Evolution. https://doi.org/10.1111/2041-210X.14099.
Jouve, S., Sarıgül, V., Steyer, J.-S., Sen, S., 2019. The first crocodylomorph from the Mesozoic of Turkey (Barremian of Zonguldak) and the dispersal of the eusuchians during the Cretaceous. Journal of Systematic Palaeontology 17, 111–128. https://doi.org/10.1080/14772019.2017.1393469.
Jurkovšek, B., Biolchi, S., Furlani, S., Kolar-Jurkovšek, T., Zini, L., Jež, J., Tunis, G., Bavec, M., Cucchi, F., 2016. Geology of the Classical Karst Region (SW Slovenia–NE Italy). Journal of Maps 12, 352–362. https://doi.org/10.1080/17445647.2016.1215941.
Kramer, G., Medem, F., 1955. Über wachstumsbedingte Proportionsänderungen bei Krokodilen. Zoologische Jahrbücher 66, 62–74.
Lee, M.S.Y., Cau, A., Naish, D., Dyke, G.J., 2014. Morphological Clocks in Paleontology, and a Mid-Cretaceous Origin of Crown Aves. Systematic Biology 63, 442–449. https://doi.org/10.1093/sysbio/syt110.
Lee, M.S.Y., Yates, A.M., 2018. Tip-dating and homoplasy: reconciling the shallow molecular divergences of modern gharials with their long fossil record. Proceedings of the Royal Society B: Biological Sciences 285, 20181071. https://doi.org/10.1098/rspb.2018.1071.
Lima, F., Santos, A., Vieira, L., Coutinho, M., 2011. Ossification sequence of skull and hyoid in embryos of Caiman yacare (Crocodylia, Alligatoridae). Iheringia. Série Zoologia 101, 161–172. https://doi.org/10.1590/S0073-47212011000200003.
Mannion, P.D., Chiarenza, A.A., Godoy, P.L., Cheah, Y.N., 2019. Spatiotemporal sampling patterns in the 230 million year fossil record of terrestrial crocodylomorphs and their impact on diversity. Palaeontology 62, 615–637. https://doi.org/10.1111/pala.12419.
Martin, J.E., 2007. New Material of the Late Cretaceous Globidontan *Acynodon iberoccitanus* (Crocodylia) from Southern France. Journal of Vertebrate Paleontology 27, 362–372.
Martin, J.E., Smith, T., de Lapparent de Broin, F., Escuillié, F., Delfino, M., 2014. Late Palaeocene eusuchian remains from Mont de Berru, France, and the origin of the alligatoroid *Diplocynodon*. Zoological Journal of the Linnean Society 172, 867–891. https://doi.org/10.1111/zoj.12195.
Martin, J.E., Delfino, M., Garcia, G., Godefroit, P., Berton, S., Valentin, X., 2016. New specimens of Allodaposuchus precedens from France: intraspecific variability and the diversity of European Late Cretaceous eusuchians. Zoological Journal of the Linnean Society 176, 607–631. https://doi.org/10.1111/zoj.12331.
Martin, J.E., Smith, T., Salaviale, C., Adrien, J., Delfino, M., 2020. Virtual reconstruction of the skull of *Bernissartia fagesii* and current understanding of the neosuchian–eusuchian transition. Journal of Systematic Palaeontology 18, 1079–1101. https://doi.org/10.1080/14772019.2020.1731722.
Motani, R., Jiang, D.-Y., Tintori, A., Rieppel, O., Chen, G.-B., You, H., 2015. First evidence of centralia in Ichthyopterygia reiterating bias from paedomorphic characters on marine reptile phylogenetic reconstruction. Journal of Vertebrate Paleontology 35, e948547. https://doi.org/10.1080/02724634.2014.948547.
Müller, G.B., Alberch, P., 1990. Ontogeny of the limb skeleton in *Alligator mississippiensis*: Developmental invariance and change in the evolution of archosaur limbs. Journal of Morphology 203, 151–164. https://doi.org/10.1002/jmor.1052030204.
Narváez, I., Brochu, C.A., Escaso, F., Pérez-García, A., Ortega, F., 2016. New Spanish Late Cretaceous eusuchian reveals the synchronic and sympatric presence of two allodaposuchids. Cretaceous Research 65, 112–125. https://doi.org/10.1016/j.cretres.2016.04.018.

Nesbitt, S.J., 2011. The early evolution of archosaurs : relationships and the origin of major clades. Bulletin of the American Museum of Natural History 352.
Palci, A., 2003. Ricostruzione Paleoambientale del Sito Fossilifero Senoniano del Villaggio del Pescatore (Trieste) (Tesi di Laurea In Paleontologia). Università degli Studi di Trieste, Trieste.
Parker, W.G., Stocker, M.R., Irmis, R.B., 2008. A New Desmatosuchine Aetosaur (Archosauria: Suchia) from the Upper Triassic Tecovas Formation (Dockum Group) of Texas. Journal of Vertebrate Paleontology 28, 692–701.
Ponce, D., Cerda, I., Desojo, J., Nesbitt, S., 2017. The osteoderm microstructure in doswelliids and proterochampsids and its implications for palaeobiology of stem archosaurs. Acta Palaeontologica Polonica 62 (4), 819–831. https://doi.org/10.4202/app.00381.2017.
Puértolas-Pascual, E., Young, M.T., Brochu, C.A., 2020. Introducing the first European symposium on the evolution of Crocodylomorpha. Zoological Journal of the Linnean Society 189, 419–427. https://doi.org/10.1093/zoolinnean/zlaa012.
Rambaut, A., Drummond, A.J., Xie, D., Baele, G., Suchard, M.A., 2018. Posterior summarization in Bayesian phylogenetics using Tracer 1.7. Systematic Biology 67, 901–904. https://doi.org/10.1093/sysbio/syy032.
Raven, T.J., Maidment, S.C.R., 2018. The systematic position of the enigmatic thyreophoran dinosaur Paranthodon africanus, and the use of basal exemplifiers in phylogenetic analysis. PeerJ 6, e4529. https://doi.org/10.7717/peerj.4529.
Rieppel, O., 1989. The hind limb of *Macrocnemus bassanii* (Nopcsa) (Reptilia, Diapsida): development and functional anatomy. Journal of Vertebrate Paleontology 9, 373–387.
Rio, J.P., Mannion, P.D., 2021. Phylogenetic analysis of a new morphological dataset elucidates the evolutionary history of Crocodylia and resolves the long-standing gharial problem. PeerJ 9, e12094. https://doi.org/10.7717/peerj.12094.
Ristevski, J., Yates, A.M., Price, G.J., Molnar, R.E., Weisbecker, V., Salisbury, S.W., 2020. Australia's prehistoric 'swamp king': revision of the Plio-Pleistocene crocodylian genus *Pallimnarchus* de Vis, 1886. PeerJ 8, e10466. https://doi.org/10.7717/peerj.10466.
Sampson, S.D., Ryan, M.J., Tanke, D.H., 1997. Craniofacial ontogeny in centrosaurine dinosaurs (Ornithischia: Ceratopsidae): taxonomic and behavioral implications. Zoological Journal of the Linnean Society 121, 293–337.
Scheyer, T.M., Desojo, J., 2011. Palaeohistology and external microanatomy of rauisuchian osteoderms (Archosauria: Pseudosuchia). Palaeontology 54, 1289–1302. https://doi.org/10.1111/j.1475-4983.2011.01098.x.
Scheyer, T.M., Sander, P.M., 2009. Bone microstructures and mode of skeletogenesis in osteoderms of three pareiasaur taxa from the Permian of South Africa. Journal of Evolutionary Biology 22, 1153–1162. https://doi.org/10.1111/j.1420-9101.2009.01732.x.
Stubbs, T.L., Pierce, S.E., Elsler, A., Anderson, P.S.L., Rayfield, E.J., Benton, M.J., 2021. Ecological opportunity and the rise and fall of crocodylomorph evolutionary innovation. Proceedings of the Royal Society B: Biological Sciences 288, 20210069. https://doi.org/10.1098/rspb.2021.0069.
Taborda, J.R.A., Cerda, I.A., Desojo, J.B., 2013. Growth curve of *Aetosauroides scagliai* Casamiquela 1960 (Pseudosuchia: Aetosauria) inferred from osteoderm histology. Geological Society, London, Special Publications 379, 413–423. https://doi.org/10.1144/SP379.19.
Tarlao, A., Tentor, M., Tunis, G., Venturini, S., 1993. Evidenze di una fase tettonica nel Senoniano inferiore dell'area del Villaggio del Pescatore (Trieste). Gortania Atti Museo Friulano Storia Naturale 23–24.
Tarlao, A., Tentor, M., Tunis, G., Venturini, S., 1995. Stop 4: Villaggio del Pescatore. Atti Museo Geologico Paleontologico Monfalcone 135–142.
Tumarkin-Deratzian, A.R., Vann, D.R., Dodson, P., 2006. Bone surface texture as an ontogenetic indicator in long bones of the Canada goose *Branta canadensis* (Anseriformes: Anatidae). Zoological Journal of the Linnean Society 148, 133–168. https://doi.org/10.1111/j.1096-3642.2006.00232.x.
Vieira, L.G., Lima, F.C., Mendonôa, S.H.S.T., Menezes, L.T., Hirano, L.Q.L., Santos, A.L.Q., 2018. Ontogeny of the Postcranial Axial Skeleton of *Melanosuchus niger* (Crocodylia, Alligatoridae). The Anatomical Record 301, 607–623. https://doi.org/10.1002/ar.23722.
von Baczko, M.B., Desojo, J.B., Ponce, D., 2019. Postcranial anatomy and osteoderm histology of *Riojasuchus tenuisceps* and a phylogenetic update on Ornithosuchidae (Archosauria, Pseudosuchia). Journal of Vertebrate Paleontology 39, e1693396. https://doi.org/10.1080/02724634.2019.1693396.
Witzmann, F., 2009. Comparative histology of sculptured dermal bones in basal tetrapods, and the implications for the soft tissue dermis. Palaeodiversity 2, 233–270.
Witzmann, F., Soler-Gijón, R., 2010. The bone histology of osteoderms in temnospondyl amphibians and in the chroniosuchian *Bystrowiella*. Acta Zoologica 91, 96–114. https://doi.org/10.1111/j.1463-6395.2008.00385.x.
Woodward Ballard, H., Horner, J., Farlow, J., 2011. Osteohistological evidence for determinate growth in the American alligator. Journal of Herpetology 45, 339–342. https://doi.org/10.1670/10-274.1.
Woodward, H.N., Horner, J.R., Farlow, J.O., 2014. Quantification of intraskeletal histovariability in *Alligator mississippiensis* and implications for vertebrate osteohistology. PeerJ 2, e422. https://doi.org/10.7717/peerj.422.

Appendix A. Supplementary data

Supplementary data to this article can be found online at https://doi.org/10.1016/j.cretres.2023.105631.